The Geological Society of America
Special Paper 542

Expansion breccias in Lower Cretaceous Apennine pelagic limestones: II. Geochemical constraints on their origin

J. Belza
Department of Chemistry, Atomic & Mass Spectrometry (A&MS) Research Unit, Ghent University, Campus Sterre, Krijgslaan 281-S12, B-9000 Ghent, Belgium

W. Alvarez
Department of Earth and Planetary Science, University of California, Berkeley, California 94720-4767, USA, and *Osservatorio Geologico di Coldigioco, Contrada Coldigioco, 62020 Frontale di Apiro, Italy*

E. Tavarnelli
Dipartimento di Scienze della Terra, Università di Siena, I-53100 Siena, Italy

F. Vanhaecke
Department of Chemistry, Atomic & Mass Spectrometry (A&MS) Research Unit, Ghent University, Campus Sterre, Krijgslaan 281–S12, B-9000 Ghent, Belgium

J.-M. Baele
Department of Geology and Applied Geology, University of Mons, Place du Parc, 20, 7000 Mons, Belgium

P. Claeys
Department of Analytical, Environmental, and Geo-Chemistry (AMGC), Vrije Universiteit Brussel, Pleinlaan 2, 1050 Brussels, Belgium

ABSTRACT

The geochemical signatures of sparry calcite-sealing expansion breccias, calcite veins, and host clasts were analyzed for their strontium ($^{87}Sr/^{86}Sr$) and oxygen and carbon ($\delta^{18}O$, $\delta^{13}C$) stable isotopic signatures. The breccias occur within the Lower Cretaceous Maiolica Formation. Related but different breccias are found in a few places in the Upper Cretaceous to Eocene Scaglia Rossa Formation of the Umbria-Marche Apennines fold-and-thrust belt (Italy). We propose hydraulic fracturing by fluid overpressure as a possible mechanism for generation of the breccias in these formations. Our data are compatible with the hypothesis of a hydraulically fractured breccia formed by cyclic buildup and rapid decompression of CO_2-rich fluids, with overpressures generated by entrapment of CO_2 by structural and stratigraphic seals. Strontium and oxygen isotope ratio data suggest that the CO_2-rich fluids may

Belza, J., Alvarez, W., Tavarnelli, E., Vanhaecke, F., Baele, J.-M., and Claeys, P., 2019, Expansion breccias in Lower Cretaceous Apennine pelagic limestones: II. Geochemical constraints on their origin, *in* Koeberl, C., and Bice, D.M., eds., 250 Million Years of Earth History in Central Italy: Celebrating 25 Years of the Geological Observatory of Coldigioco: Geological Society of America Special Paper 542, p. 251–269, https://doi.org/10.1130/2019.2542(13). © 2019 The Geological Society of America. All rights reserved. For permission to copy, contact editing@geosociety.org.

have originated from carbonate metasomatism of the mantle, resulting from subduction of carbonate-rich lithologies constituting the downgoing slab. This is consistent with previous conceptual models inferring that in the central part of the Northern Apennines, which is characterized by thick continental crust, CO_2-rich fluids derived from mantle metasomatism would become trapped in structural seals, creating high fluid overpressures.

INTRODUCTION

This chapter gives sample descriptions and isotopic data for unusual breccias in the Maiolica Formation, a Lower Cretaceous pelagic limestone in the Umbria-Marche Apennines of central Italy. This limestone is part of the Jurassic to Oligocene Umbria-Marche sequence of limestones, marls, and cherts, which were mostly deposited in moderately deep water and deformed into a fold-and-thrust belt during the Neogene. The stratigraphy and its geological setting have been described by Alvarez (1989a, 1989b, 2009), Cresta et al. (1989), Montanari and Koeberl (2000), and Barchi et al. (2001). Extensive field observations and petrography are discussed in the companion paper (Alvarez et al., this volume, Chapter 12), where the breccias are hypothesized to have formed by expansion, driven by a CO_2-rich fluid. This paper investigates the source of the fluids that drove the fragmentation and deposited the calcite in veins and in between the breccia clasts.

SAMPLES AND METHODS

Samples were taken from several localities along the breccia walls at Monte Cucco and Monte Catria. A list with coordinates and description of the localities is given in Table 1, along with the results of isotopic analysis. Furthermore, in a companion paper (Belza et al., this volume), samples from Maiolica Formation limestones were taken along a large stratigraphic interval at different localities (Frontale [FRO], Presale [PRE], and Monte Acuto [MMA]) to obtain a stratigraphic record of the $^{87}Sr/^{86}Sr$ ratios of the Maiolica Formation host rocks. Furthermore, the Sr isotope record was carefully tied to a magnetostratigraphically and biostratigraphically calibrated time scale. The results of this study indicate that the $^{87}Sr/^{86}Sr$ record accurately follows the trend of the marine $^{87}Sr/^{86}Sr$ reference curve, although individual Sr isotope ratio values are uniformly increased by 0.00007 with respect to their stratigraphic position.

Analytical Protocols: Geochemical Analysis

Samples were cut with a diamond saw to expose a fresh surface displaying the breccia structures. Subsequently, the slab surfaces were cleaned with pressurized air and acetone to remove surface contaminants. Next, a dental drill (with a tungsten-carbide drill bit) was used to scrape off a small portion of the surface. This was done to further clean the slab surface and to "precontaminate" the drill bit with the sample powder. After that, the drill bit was cleaned with pressurized air, and sample powder from the calcite veins, host rocks, and calcite fills between the breccia clasts was carefully drilled out and transferred to clean vials. In between drilling of different samples, the dental drill and drill bits were cleaned with pressurized air and ultrapure 18.2 MΩ·cm water to avoid cross-contamination. The vials were wrapped in parafilm before further analysis.

Sr Isotopic Analysis

Depending on the size of the sample and the amount of powder that could be recovered by drilling, between 10 and 100 mg samples of powder were weighed in precleaned Teflon® beakers. Next, 1 *M* HCl was added to dissolve the samples. Along with the samples, one National Institute of Standards and Technology (NIST) SRM 987 standard, several procedure blanks, and sample duplicates were dissolved as well.

Almost no visible residue was present after dissolution, and the sample solutions appeared clear. To fully eliminate any possible contribution from radiogenic ^{87}Sr leached from clay fractions in the following steps involving concentrated acid attack, the solutions were centrifuged. After centrifugation, clear supernatant solutions were pipetted off and transferred to clean Savillex® vials. Next, the solutions were evaporated to near-dryness on a hotplate at 70 °C and redissolved in 2 mL of 7 *M* HNO_3.

Because of the lack of an appropriate calcite reference material yielding a certified $^{87}Sr/^{86}Sr$ signature, two certified silicate geochemical reference standards (basalt standard BE-N and microgabbro PM-S, obtained from the Centre de Recherches Pétrographiques et Géochimiques, Nancy, France) were prepared following a different digestion protocol: ~100 mg samples of powder were accurately weighed in clean Savillex beakers and digested by addition and subsequent evaporation of (1) HF:HNO_3 (28 *M* HF, 24 *M* HNO_3, in a ratio of 2:4), (2) aqua regia, (3) 14 *M* HNO_3, and (4) 14 *M* HNO_3. Finally, the sample was redissolved in 7 *M* HNO_3.

Major- and Minor-Element Analysis

Sr, Ca, Mg, Mn, and Fe contents of selected samples were measured using inductively coupled plasma–optical emission spectrometry (ICP-OES) using a Spectro Arcos instrument at Ghent University, Ghent, Belgium. Six procedure duplicates (separately digested) were analyzed in the same sequence, yielding good external reproducibility (relative standard deviation [RSD] = 5.5%, 2.9%, and 2.2% for Mn, Fe, and Mg, respectively). Detection limits for Mn, Fe, and Mg were 0.042,

TABLE 1. Sr, O, AND C ISOTOPIC ANALYSIS RESULTS FOR BRECCIA CLASTS, VEINS, AND CALCITE FILL BRECCIA

Formation	Age	Section/locality	Collected	Sample ID	Component	$^{87}Sr/^{86}Sr$	SD*	RSD†	Sr (μg/g)	$\delta^{13}C$§ (‰)	$\delta^{18}O$§ (‰)
Maiolica	L. Cret.	Colle gli Scogli veins	2012 (JB, WA)	CgS/12 A-18.1	Vein	0.70759	0.00007	0.009	142	1.73	2.40
Maiolica	L. Cret.	Colle gli Scogli veins	2012 (JB, WA)	CgS/12 A-18.2	Clast	0.70755	0.00008	0.011	158	1.77	–2.06
Maiolica	L. Cret.	Colle gli Scogli veins	2012 (JB, WA)	CgS/12 C-15.1	Vein	0.70760	0.00004	0.005	176	1.67	2.46
Maiolica	L. Cret.	Colle gli Scogli veins	2012 (JB, WA)	CgS/12 C-15.2	Clast	0.70754	0.00004	0.005	162	1.72	–1.92
Maiolica	L. Cret.	Colle gli Scogli breccia	2012 (JB, WA)	CgS/12 F+4.1	Calcite fill breccia	0.70761	0.00005	0.007	137	1.85	2.75
Maiolica	L. Cret.	Colle gli Scogli breccia	2012 (JB, WA)	CgS/12 F+4.2	Clast	0.70759	0.00006	0.008	151	1.79	–2.26
Maiolica	L. Cret.	Colle gli Scogli breccia	2012 (JB, WA)	CgS/12 F+4.3	Clast	0.70755	0.00005	0.007	152	1.76	–2.28
Massiccio	L. Jur.	Gola del Corno	2012 (JB, WA)	GdC-1B	Calcite fill breccia	0.70770	0.00004	0.006	242	2.09	–5.49
Massiccio	L. Jur.	Gola del Corno	2012 (JB, WA)	GdC-1B-2	Calcite fill breccia	0.70771	0.00005	0.007	201	2.42	–1.00
Massiccio	L. Jur.	Gola del Corno	2012 (JB, WA)	GdC-2B-1	Clast	0.70754	0.00005	0.008	130	2.65	–1.90
Massiccio	L. Jur.	Gola del Corno	2012 (JB, WA)	GdC-2B-2	Vein/calcite fill breccia	0.70765	0.00004	0.006	98	2.24	–3.89
Massiccio	L. Jur.	Gola del Corno	2012 (JB, WA)	GdC-2B-3	Calcite fill breccia	0.70779	0.00006	0.009	130	1.90	–2.62
Massiccio	L. Jur.	Gola del Corno	2012 (JB, WA)	GdC-2B-3.2	Calcite fill breccia	0.70775	0.00005	0.007	148	1.86	–2.57
Massiccio	L. Jur.	Gola del Corno	2012 (JB, WA)	GdC-3B-1	Calcite fill breccia	0.70774	0.00004	0.006	170	1.84	–2.57
Massiccio	L. Jur.	Gola del Corno	2012 (JB, WA)	GdC-3B-2.1	Clast	0.70752	0.00004	0.006	129	2.61	–1.51
Massiccio	L. Jur.	Gola del Corno	2012 (JB, WA)	GdC-3B-2.2	Clast	0.70758	0.00006	0.008	139	2.76	–1.57
Massiccio	L. Jur.	Gola del Corno	2012 (JB, WA)	GdC-3B-3	Calcite fill breccia	0.70778	0.00004	0.006	157	1.99	–4.69
Massiccio	L. Jur.	Gola del Corno	2012 (JB, WA)	GdC-4B-1	Clast	0.70758	0.00008	0.011	120	2.37	–1.42
Massiccio	L. Jur.	Gola del Corno	2012 (JB, WA)	GdC-4B-2	Calcite fill breccia	0.70769	0.00009	0.012	48.6	2.65	2.45
Maiolica	L. Cret.	Frontale road breccia	2012 (JB, WA)	Nap. U11-62.1	Clast	0.70754	0.00005	0.007	138	1.33	–1.55
Maiolica	L. Cret.	Frontale road breccia	2012 (JB, WA)	Nap. U11-62.2	Calcite fill breccia	0.70769	0.00006	0.009	124	1.90	1.68
Scaglia Rossa	U. Cret.	Balzone del Lupo	2012 (JB, WA)	U12-12-1B-1	Clast	0.70737	0.00005	0.007	339	2.20	–2.43
Scaglia Rossa	U. Cret.	Balzone del Lupo	2012 (JB, WA)	U12-12-1B-2	Vein/calcite fill breccia	0.70743	0.00003	0.005	302	2.27	–0.26
Scaglia Rossa	U. Cret.	Balzone del Lupo	2012 (JB, WA)	U12-12-6-1	Calcite fill breccia	0.70751	0.00005	0.007	363	2.01	–1.62
Scaglia Rossa	U. Cret.	Balzone del Lupo	2012 (JB, WA)	U12-12-6-2	Clast	0.70742	0.00006	0.008	352	2.00	–1.79
Scaglia Rossa	U. Cret.	Fault on Sigillo–Monte Cucco Road	2012 (JB, WA)	U12-28-1B-1	Clast	0.70747	0.00005	0.007	490	2.27	–2.32
Scaglia Rossa	U. Cret.	Fault on Sigillo–Monte Cucco Road	2012 (JB, WA)	U12-28-1B-2	Calcite fill breccia	0.70757	0.00006	0.008	277	2.22	0.15
Scaglia Rossa	U. Cret.	Fault on Sigillo–Monte Cucco Road	2012 (JB, WA)	U12-28-4-1	Calcite fill breccia	0.70754	0.00006	0.008	224	2.48	0.63
Scaglia Rossa	U. Cret.	Fault on Sigillo–Monte Cucco Road	2012 (JB, WA)	U12-28-4-2	Clast	0.70743	0.00006	0.009	360	2.53	–2.36
Maiolica	L. Cret.	Colle gli Scogli breccia	2011 (WA)	U11-28-1	Clast	0.70755	0.00007	0.009	n.a.	1.74	–1.96
Maiolica	L. Cret.	Colle gli Scogli breccia	2011 (WA)	U11-28-2	Calcite fill breccia	0.70765	0.00006	0.009	n.a.	2.02	2.64
Maiolica	L. Cret.	Colle gli Scogli breccia	2011 (WA)	U11-28-3	Clast	0.70759	0.00006	0.008	n.a.	1.75	–1.74
Maiolica	L. Cret.	Colle gli Scogli breccia	2011 (WA)	U11-28-4	Clast	0.70760	0.00005	0.007	n.a.	1.75	–1.74
Maiolica	L. Cret.	Colle gli Scogli breccia	2011 (WA)	U11-28-5	Calcite fill breccia	0.70770	0.00005	0.007	n.a.	2.25	1.37
Maiolica	L. Cret.	Fonte della Vernosa breccia	2011 (WA)	U11-144-6	Clast	0.70756	0.00005	0.007	n.a.	1.54	–2.72
Maiolica	L. Cret.	Fonte della Vernosa breccia	2011 (WA)	U11-144-7	Vein	0.70761	0.00007	0.010	n.a.	1.55	–4.26
Maiolica	L. Cret.	Fonte della Vernosa breccia	2011 (WA)	U11-144-8	Calcite fill breccia	0.70770	0.00007	0.010	n.a.	2.40	3.48
Maiolica	L. Cret.	Fonte della Vernosa breccia	2011 (WA)	U11-144-9	Vein	0.70764	0.00006	0.009	n.a.	1.48	–4.73
Maiolica	L. Cret.	Fonte della Vernosa breccia	2011 (WA)	U11-144-10	Clast	0.70756	0.00006	0.008	n.a.	1.53	–3.01
Maiolica	L. Cret.	Fonte della Vernosa breccia	2011 (WA)	U11-144-11	Vein	0.70770	0.00006	0.008	n.a.	1.71	–5.45
Maiolica	L. Cret.	Fonte della Vernosa breccia	2011 (WA)	U11-144-12	Calcite fill breccia	0.70773	0.00004	0.006	n.a.	2.40	3.76
Maiolica	L. Cret.	Fonte della Vernosa breccia	2011 (WA)	U11-144-13	Clast	0.70750	0.00006	0.008	n.a.	1.51	–2.61
Maiolica	L. Cret.	Fonte della Vernosa breccia	2011 (WA)	U11-144-14	Vein	0.70757	0.00006	0.009	n.a.	1.65	–3.92
Maiolica	L. Cret.	Fonte della Vernosa breccia	2011 (WA)	U11-144-15	Vein	0.70765	0.00005	0.007	n.a.	1.62	–4.92
Maiolica	L. Cret.	Fonte della Vernosa breccia	2011 (WA)	U11-144-16	Calcite fill breccia	0.70771	0.00005	0.007	n.a.	2.29	2.11

(*Continued*)

TABLE 1. Sr, O, AND C ISOTOPIC ANALYSIS RESULTS FOR BRECCIA CLASTS, VEINS, AND CALCITE FILL BRECCIA (*Continued*)

Duplicates for Sr isotopic analyses

Formation	Age	Section/locality	Sample ID	Lithology	$^{87}Sr/^{86}Sr$	SD*	RSD†
Massiccio	L. Jur.	Gola del Corno	CdC-3B-1	Calcite fill breccia	0.70774	0.000040	0.006
Massiccio	L. Jur.	Gola del Corno	CdC-3B-1bis	Calcite fill breccia	0.70776	0.000049	0.007
Scaglia Rossa	U. Cret.	Balzone del Lupo	U12-12-1B-2bis	Calcite fill breccia/vein	0.70746	0.000060	0.008
Scaglia Rossa	U. Cret.	Balzone del Lupo	U12-12-1B-2	Calcite fill breccia/vein	0.70743	0.000034	0.005
Maiolica	L. Cret.	Colle gli Scogli breccia	Cgs/12 A-18.2	Clast	0.70755	0.000078	0.011
Maiolica	L. Cret.	Colle gli Scogli breccia	CgS/12 A-18.2bis	Clast	0.70759	0.000049	0.007
Maiolica	L. Cret.	Fonte della Vernosa breccia	U11-144-8	Calcite fill breccia	0.70770	0.000067	0.010
Maiolica	L. Cret.	Fonte della Vernosa breccia	U11-144-8bis	Calcite fill breccia	0.70769	0.000048	0.007
Maiolica	L. Cret.	Fonte della Vernosa breccia	U11-144-12	Calcite fill breccia	0.70773	0.000043	0.006
Maiolica	L. Cret.	Fonte della Vernosa breccia	U11-144-12bis	Calcite fill breccia	0.70774	0.000065	0.009
Maiolica	L. Cret.	Fonte della Vernosa breccia	U11-144-14	Vein	0.70757	0.000063	0.009
Maiolica	L. Cret.	Fonte della Vernosa breccia	U11-144-14bis	Vein	0.70764	0.000052	0.007
Maiolica	L. Cret.	Fonte della Vernosa breccia	U11-144-15	Vein	0.70765	0.000053	0.007
Maiolica	L. Cret.	Fonte della Vernosa breccia	U11-144-15bis	Vein	0.70765	0.000056	0.008

Reference standards#

Lithology	Sample type	Sample ID	$^{87}Sr/^{86}Sr$ measured	SD*	RSD†	Reference value (GEoREM) $^{87}Sr/^{86}Sr$
Micro-gabbro	Geostandard#	Standard PM-S	0.70465	0.000052	0.00734	0.704596
Basalt	Geostandard#	Standard BE-N	0.70385	0.000047	0.00668	0.703791 –0.70403

Note: L.—Lower; U.—Upper; Cret—Cretaceous; Jur—Jurassic; JB—J. Belza; WA—W. Alvarez; n.a.—not analyzed. For the duplications, a standard deviation of the mean of all pairs was calculated to be SD = 0.000023, showing excellent reproducibility.

*SD—standard deviation.

†RSD—relative standard deviation.

§All delta values are reported against Vienna Peedee belemnite (PDB) standard.

#Measured values for geostandards obtained from Le Centre de Recherches Pétrographiques et Géochimiques (CRPG) are in excellent agreement with reported values.

0.045, and 0.093 µg g^{-1}, respectively. Analyses are reported in Table 2.

To isolate the Sr fraction from its concomitant matrix, sample solutions were loaded onto BioRad columns prepacked with a 30 µm porous polyethylene bed and filled with 400 µL of the commercially available strontium-specific extraction chromatographic resin Sr spec™. After loading of the sample digest, dissolved in 7 *M* HNO_3, onto the resin, the resin was rinsed with 5 mL of 7 *M* HNO_3 solution to remove matrix elements, while the resin retained the Sr. The purified Sr fraction was subsequently stripped off the resin in a quantitative manner through rinsing with 6 mL of 0.05 *M* HNO_3. Details of the procedure can be found in De Muynck et al. (2009). After isolation, Sr concentrations were checked to assess full quantitative recovery.

The $^{87}Sr/^{86}Sr$ ratios were measured using a Neptune multi-collector–inductively coupled plasma–mass spectrometry (MC-ICP-MS) instrument at the Department of Chemistry, Ghent University. All samples were run in a sample-standard bracketing sequence with 100 µg/L of Sr isotopic standard solution of NIST SRM 987 $SrCO_3$. The Sr content of the sample solutions and the standard were matched within ±10% to avoid any effect from the analyte content on the extent of instrumental mass discrimination. After every run, the sample introduction system was rinsed thoroughly with 2% HNO_3 to minimize memory effects. Mass bias was mathematically corrected using internal normalization to $^{86}Sr/^{88}Sr = 0.1194$ by the exponential fractionation law.

The mean $^{87}Sr/^{86}Sr$ ratio obtained for NIST SRM 987 $SrCO_3$ was 0.710307 ± 0.000024 (2σ, $N = 15$). This is in agreement with the accepted $^{87}Sr/^{86}Sr$ ratio of 0.710248 ± 0.000011 (2 standard deviation [SD]) for this reference material (Thirlwall, 1991). The internal precision (reported as the standard deviation, SD) for each reference sample was between ±0.000042 and ±0.000079. A better estimate of the precision was also provided by calculating the standard deviation of the mean of all pairs of duplicate analyses of the samples. For seven pairs (14 duplicate analyses), the standard deviation of the mean of all (duplicate) pairs was found to be 0.000024, demonstrating excellent reproducibility. All strontium isotopic data are reported in Table 1.

C and O Isotopic Analysis

Carbon and oxygen isotope ratios were measured both with a Kiel-III device coupled to a Thermo Delta plus XL isotope ratio mass spectrometer, and a NuCarb automated carbonate preparation device coupled to a Nu Perspective isotope ratio mass spectrometer, both in operation at Vrije Universiteit Brussel. Small quantities of carbonate powder were reacted with orthophosphoric acid at a temperature of 75 °C, and the CO_2 thus generated was collected with cryotraps. Every set of six samples was bracketed by a calcite standard (NBS-19 with $\delta^{18}O = -2.20‰ \pm 0.01‰$ and $\delta^{13}C = +1.95‰ \pm 0.02‰$, or NCM with $\delta^{18}O = -1.9‰$ and $\delta^{13}C = +2.09‰$). Moreover, every sample was analyzed three to four times on different measurement days to assess reproducibility. The $\delta^{13}C$ and $\delta^{18}O$ values reported in Table 1 are the average of those replicates. All analyses are reported in Table 1.

Cathodoluminescence

Cathodoluminescence (CL) imaging was performed at University of Mons, Mons, Belgium, using a cold cathode system

TABLE 2. Mg, Fe, AND Mn CONCENTRATIONS OF SELECTED BRECCIA CLASTS, CALCITE BRECCIA FILL, AND VEINS

Age	Section/locality	Collected	Sample ID	Component	Mn (µg/g)	Fe (µg/g)	Mg (µg/g)
L. Cret.	Colle gli Scogli veins	2012 (JB, WA)	CgS/12 A-18.1	Vein	291	215	1826
L. Cret.	Colle gli Scogli veins	2012 (JB, WA)	CgS/12 A-18.2	Clast	304	544	1875
L. Cret.	Colle gli Scogli veins	2012 (JB, WA)	CgS/12 C-15.1	Vein	284	346	1403
L. Cret.	Colle gli Scogli veins	2012 (JB, WA)	CgS/12 C-15.2	Clast	306	537	1898
L. Cret.	Colle gli Scogli breccia	2012 (JB, WA)	CgS/12 F+4.1	Calcite fill breccia	203	89	1665
L. Cret.	Colle gli Scogli breccia	2012 (JB, WA)	CgS/12 F+4.3	Clast	226	440	1866
L. Cret.	Colle gli Scogli breccia	2012 (JB, WA)	CgS/12 F+4.3bis	Clast	247	450	1946
L. Cret.	Colle gli Scogli breccia	2012 (JB, WA)	CgS/12 F+4.3tris	Clast	230	452	1901
L. Jur.	Gola del Corno	2012 (JB, WA)	GdC-3B-2.2	Clast	73	83	3016
L. Jur.	Gola del Corno	2012 (JB, WA)	GdC-3B-3	Calcite fill breccia	67	94	2149
L. Jur.	Gola del Corno	2012 (JB, WA)	GdC-4B-1	Clast	68	103	2415
L. Cret.	Frontale road breccia	2012 (JB, WA)	Nap. U11-62.1	Clast	226	555	1590
L. Cret.	Frontale road breccia	2012 (JB, WA)	Nap. U11-62.2	Calcite fill breccia	344	692	1172
U. Cret.	Fault on Sigillo–Monte Cucco Road	2012 (JB, WA)	U12-28-4-1	Calcite fill breccia	414	552	953
L. Cret.	Colle gli Scogli breccia	2011 (WA)	U11-28-2	Calcite fill breccia	419	254	3240
L. Cret.	Colle gli Scogli breccia	2011 (WA)	U11-28-3	Clast	276	536	1844
L. Cret.	Fonte della Vernosa breccia	2011 (WA)	U11-144-7	Vein	279	396	1706
L. Cret.	Fonte della Vernosa breccia	2011 (WA)	U11-144-8	Calcite fill breccia	396	425	1813
L. Cret.	Fonte della Vernosa breccia	2011 (WA)	U11-144-10	Clast	379	995	1139
L. Cret.	Fonte della Vernosa breccia	2011 (WA)	U11-144-13	Clast	257	532	1357

Note: L.—Lower; U.—Upper; Cret—Cretaceous; Jur—Jurassic; JB—J. Belza; WA—W. Alvarez.

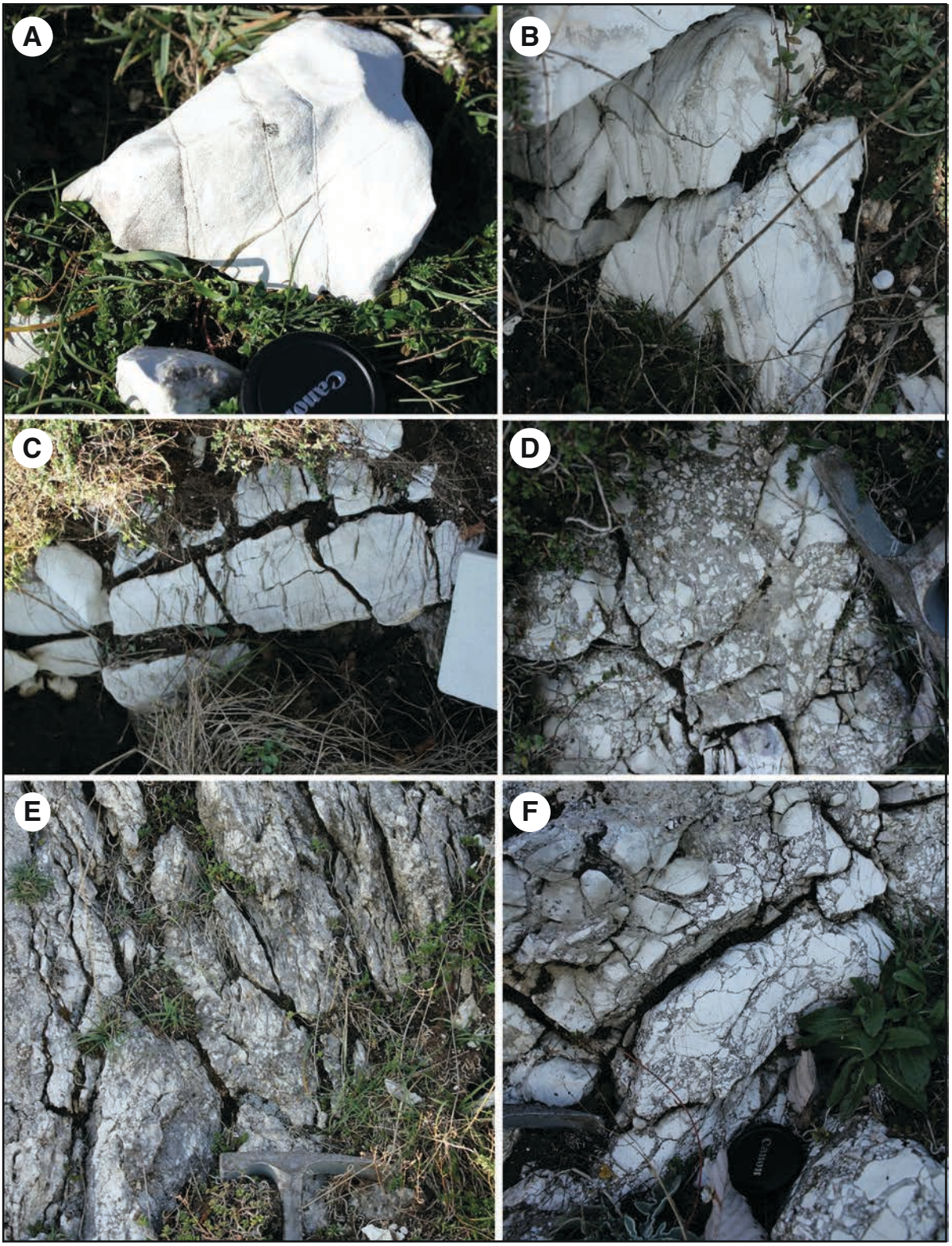

Figure 1. Maiolica lithologies along the Colle gli Scogli transect (Alvarez et al. this volume). (A–C) Parallel, discrete veins in Maiolica limestone west of the solution tectonite. (D, F) Expansion breccia in Maiolica, east of the solution tectonite. (E) The solution tectonite, marking a right-lateral, north-south strike-slip fault. The sparry calcite in the veins and the calcite cementing the breccia have the same $^{87}Sr/^{86}Sr$ and $\delta^{18}O$ and $\delta^{13}C$ isotopic signatures, indicating a common source for the cementing fluids.

(model Mk5, Cambridge Image Technology, UK) operated at 15 kV and 500 µA acceleration voltage and beam current, respectively. With these settings, the unfocused electron beam has a current density of 8 µA/mm^2. CL micrographs were captured with a Peltier-cooled digital color camera (model Infinity 4, Lumenera, Canada) set with a few to a few tens of milliseconds exposure time depending on CL intensity and magnification used (5× or 20×).

RESULTS

The samples have been described in detail in our companion paper (Alvarez et al., this volume). Short descriptions will briefly be reviewed here. Samples from the Monte Cucco breccia wall localities display a spectrum from vein networks to expansion breccias. At the Colle gli Scogli transect, described in our companion paper (Alvarez et al., this volume), expansion breccias consist of a jigsaw puzzle fit of sharp, angular clasts in a coarse calcite fill. Westward, the Maiolica carbonates are not affected by brecciation, but instead they are cut by parallel, discrete calcite veins, perpendicular to the bedding (Figs. 1A and 1B). Both the calcite deposited in the discrete veins and the calcite fill surrounding the breccia clasts display similar Sr, O, and C isotopic signatures (Table 1). Sr concentrations in the calcite fill are similar to the brecciated host clasts, while Fe and Mn contents in the calcite fill are slightly decreased compared to the brecciated host clasts.

In addition to the Colle gli Scogli breccia body in the Maiolica Formation in the Monte Cucco–Sigillo area, we also sampled a fault-related breccia along the Monte Cucco–Sigillo area (Sigillo–Monte Cucco road), and a breccia occurring in extension fractures at Balzone del Lupos. Both breccia bodies occur in the Scaglia Rossa Formation. Neither of these is an expansion breccia. However, in these two localities and at Colle gli Scogli, the calcite filling the voids between the brecciated clasts and the calcite veins display the same Sr and $\delta^{18}O$ isotopic signature (Table 1): They are both enriched in ^{87}Sr ($^{87}Sr/^{86}Sr$ ~0.7077 for the Maiolica Formation and ~0.7075 for the Scaglia Rossa) with respect to the host rock ($^{87}Sr/^{86}Sr$ ~0.7075 for the Maiolica Formation and ~0.7074 for the Scaglia Rossa Formation). They have positive $\delta^{18}O$ ($\delta^{18}O$ ~+1.5‰ to +4‰) values in the calcite veins and sparry calcite breccia fill, compared to negative values around ~–2‰ for the host Maiolica and Scaglia Rossa limestone. Furthermore, the calcite breccia fill is slightly enriched in $\delta^{13}C$ compared to the host clasts. This suggests that the fluids depositing the calcite likely had a common source in all three localities.

At the Gola del Corno and Fonte della Vernosa localities (Monte Catria breccia wall), we observed at least two generations of calcite, not just one (Fig. 2). The first generation of calcite are calcite veins, which crosscut the breccia fragments but terminate at the fragments edges, indicating they predate the brecciation. These veins are strongly depleted in ^{18}O but enriched in ^{87}Sr compared to the host clasts. The second generation of calcite

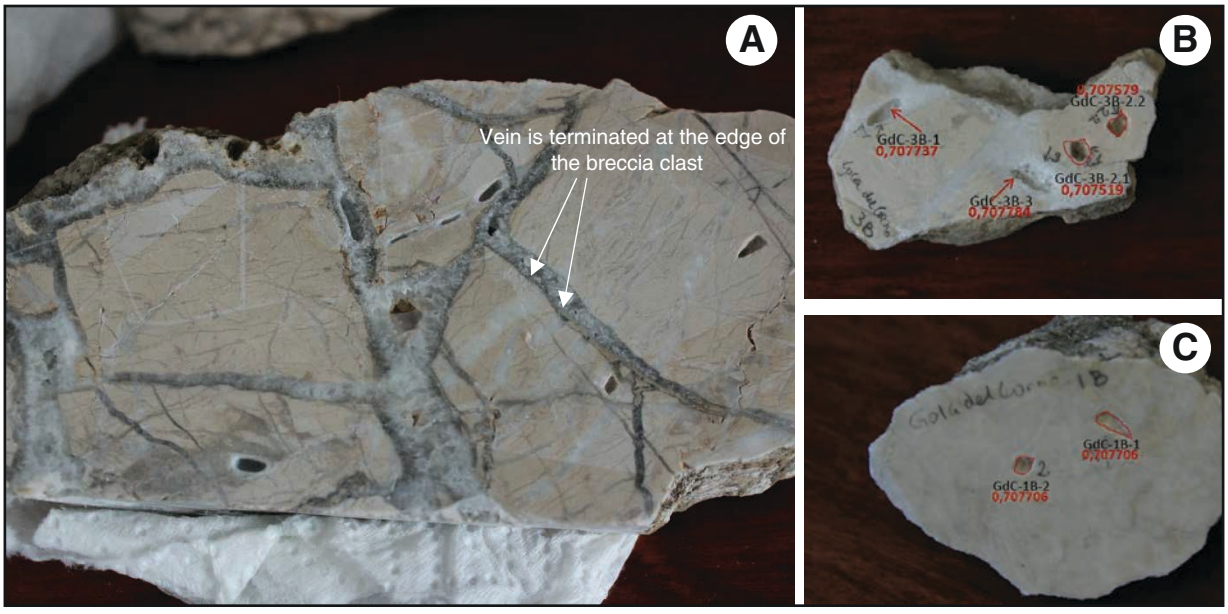

Figure 2. Photographs of expansion breccias depicting localities of drilled powders for isotopic analysis. (A) Fonte delle Vernosa locality. Calcite-filled veins are crosscut by a second generation of calcite filling voids between the angular breccia host-rock clasts. (B–C) Samples from the Gola del Corno locality. In B, clasts are "floating" in a sparry calcite cement. The clasts are crosscut by an earlier generation of calcite veins. Progressive alteration of the Gola del Corno samples toward a marble-like texture was noted.

is the calcite deposited in between the breccia fragments. This calcite breccia fill shows the same $^{86}Sr/^{86}Sr$ and $\delta^{18}O$ signature as those from the Colle gli Scogli (breccia wall exposure at Monte Cucco), yielding both elevated $^{87}Sr/^{86}Sr$ and $\delta^{18}O$. Cross-plots of $^{87}Sr/^{86}Sr$ versus $\delta^{18}O$ (Fig. 3) for breccia host clasts, veins, and breccia calcite fill demonstrate these observations.

Sr, Mn, Fe, and Mn concentrations in the calcite filling the voids between the breccia fragments, and the calcite in the parallel veins are quite similar to the brecciated host clasts, although Fe, Mn, and Mg contents in the calcite fill are slightly depleted with respect to the host rock. On average, Mn, Fe, and Mg contents are low: Mn contents typically do not exceed 400 μg g^{-1}, while Fe and Mg contents are below 1000 and 3200 μg g^{-1}, respectively.

Petrographic Textures

Most of the calcite fill observed in the parallel veins and filling the voids in between the breccia fragments is coarse and appears blocky, rather than elongate fibrous or fibrous. No mechanical twinning appears to have affected the calcite.

CL imaging revealed that the calcite fill exhibits sector zoning and fine banding resembling growth zoning (Fig. 4). However, the fine banding is different from the widespread oscillatory zoning (e.g., Shore and Fowler, 1996), mostly because the zoning is not continuous and lacks the typical oscillations between alternating bands. It seems to affect specific sectors only, and even in these sectors, the banding is discontinuous and consists of a more or less regular stacking of arrowhead or flat-triangular blocks, which could relate to sector zoning resulting from abrupt changes in relative growth rate between different crystallographic calcite forms. The zoning appears very faint; the blocky calcite fill shows an overall dull and rather homogeneous CL texture. Interestingly, this CL texture is ubiquitous and seems to be consistent for calcite filling in both parallel veins and breccia networks, in all localities studied.

The zoning observed under CL is very different from deformation-induced twin lamellae (e.g., Burkhard, 1993), which may be curved and discontinuous but are not restricted to specific sectors, and which appear as a more regular banding, often with cross geometry, and do not exhibit the typical arrowhead or triangular morphologies we observed consistently in this study.

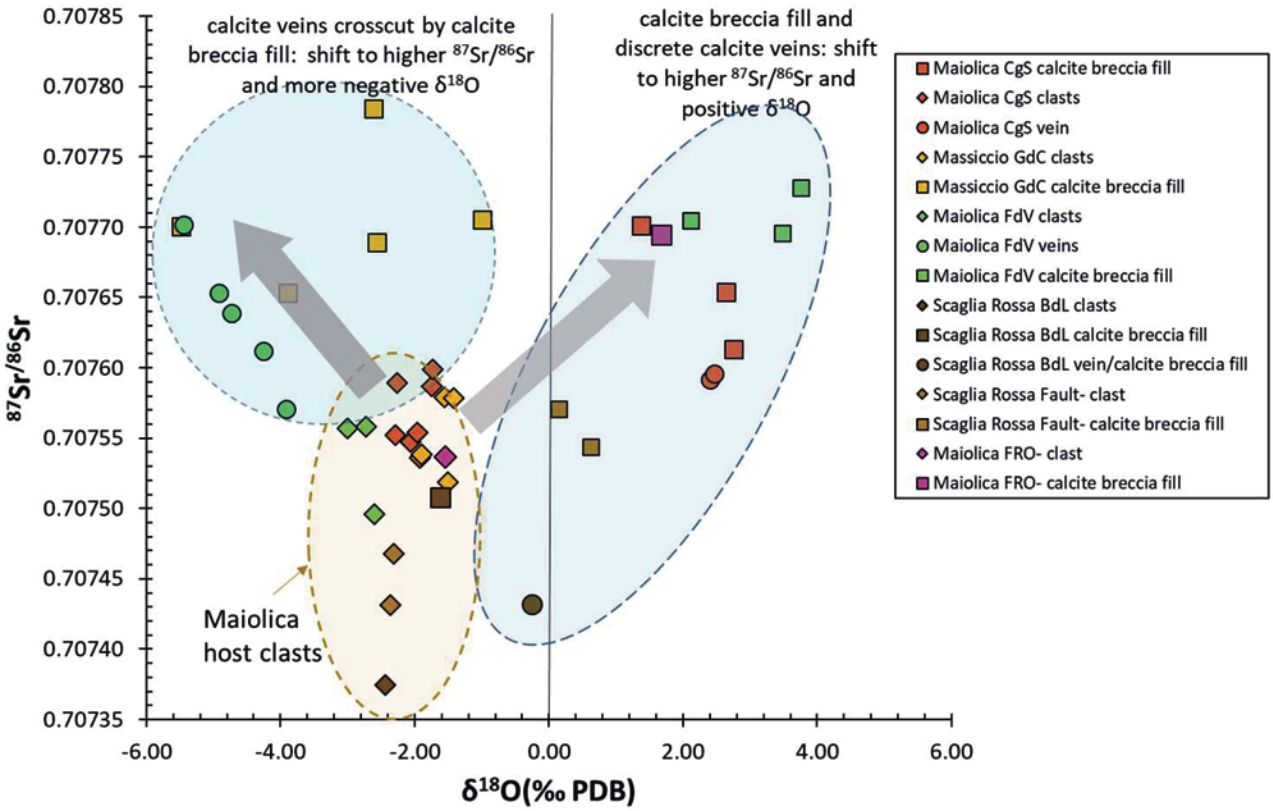

Figure 3. Cross-plot of $^{87}Sr/^{86}Sr$ vs. $\delta^{18}O$. Discrete calcite veins and calcite in the breccia calcite fill are shifted toward positive $\delta^{18}O$ and higher $^{87}Sr/^{86}Sr$ values in all localities sampled. Earlier generations of calcite veins, which are crosscut by the breccia calcite fill, are shifted toward negative $\delta^{18}O$ values only at the Gola del Corno and Fonta delle Vernosa (GdC, FdV) localities. Abbreviations: CgS—Colle gli Sogli, FRO—Frontale, BdL—Balzone delle Lupo, PDB—Peedee belemnite.

DISCUSSION

Origin of Fracturing and Brecciation: Constraints from Textural Relations

The (1) angular-shaped clasts of the breccia, fitted in a jigsaw puzzle suggesting limited transport of the fragments, (2) the three-dimensional volumetric expansion of the breccia, and (3) the widespread calcite cementation of large extensional veins and calcite breccia fill are typical features of hydraulic breccias. Such breccias are created by explosive, hydraulic expansion of a fractured host rock.

Hydraulic fracturing is caused by high fluid pressures and can be expressed by

$$P > \sigma_3 + T, \quad (1)$$

where P is the fluid pressure, σ_3 is minimum principal stress, and T is the tensile strength of the rocks, suggesting that a hydraulic fracture is formed when the fluid pressure exceeds both the minimum principal stress, σ_3, and the tensile strength of the rocks, T. As such, hydrofractures or veins will open in the direction of the minimum principal stress, σ_3, exhibiting a marked alignment normal to this direction. The formation of hydraulic fractures (veins) versus brecciation has been summarized by Cosgrove (1995). He argued that the orientation and spatial organization of hydraulic fractures in rocks and sediments are determined by (1) the magnitude of the differential stress, (2) the orientation of the principal stress axes, and (3) the intrinsic properties of the rocks, particularly their cohesive strength. Depending on the values of these various parameters, the expression of hydraulic fracturing in a rock or sediment can be extremely varied, ranging from conjugate shear fractures

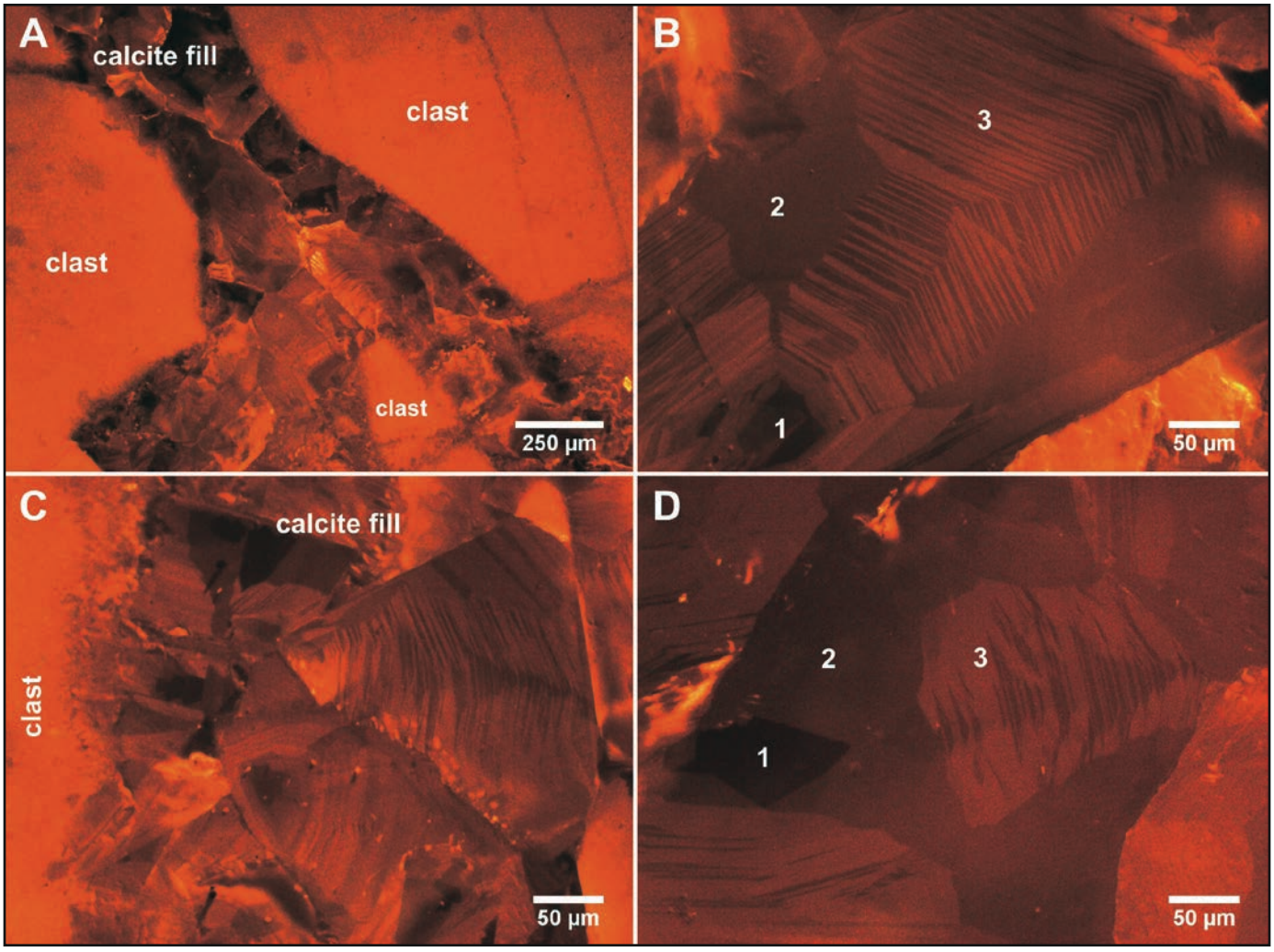

Figure 4. Cathodoluminescence (CL) imaging of the expansion breccia. (A) Overview showing the blocky structure of the calcite fill, which exhibits an overall duller CL than the clasts. (B–D) Calcite crystals with discontinuous banding similar to fir-tree zoning (Raven and Dickson, 1989), which appears as arrays of arrowhead and flat triangular blocks. 1 and 2—crystal sectors with homogeneous CL; 3—crystal sectors affected by fir-tree zoning.

through parallel tension fractures to randomly oriented fractures and fluidized sediments (Cosgrove, 1995).

According to Cosgrove (1995), tensile fractures will form parallel to the maximum principal compressive stress, σ_1. They open in the direction of the minimum principal stress, σ_3. As such, in a stress state that is characterized by large differential stress, there is a definite direction of easy opening for the tensile fractures: parallel to σ_3. The tensile fractures would therefore exhibit a marked alignment normal to this direction. However, when the differential stress become progressively smaller, the preferred orientation of tensile fractures will decrease. In the case of a hydrostatic stress field, the normal stress across all planes is the same, and there is therefore no direction of relatively easy opening for the tensile fractures. Thus, the fractures will show no preferred orientation, and, if they are sufficiently closely spaced and developed, they will produce a brecciation of the rock (Cosgrove, 1995).

The veins around the breccia walls are parallel to the walls (vertically aligned), suggesting that the direction of minimum principal stress, σ_3, was horizontal, as in most extensional settings. Contrary to the veins, the breccia in the central part of the walls exhibited a triaxial volumetric expansion, which is consistent with a hydrostatic stress field. In this case, the fractures will be extensional and multidirectional, producing a breccia (Fig. 5; Cosgrove, 1995). As such, the difference in the degree of fracturing (parallel veins vs. explosion breccias) across the breccia walls in this study reflects the evolution in stress and fluid pressure state (Fig. 5).

Hydrofracturing provides high-permeability pathways that allow the high-velocity fluid to escape and lower the fluid pressure toward hydrostatic levels. Both temperature and pressure drops promote chemical disequilibrium and cause precipitation of minerals from the fluid that is flowing through the fractures (Vrolijk, 1987; Eisenlohr et al., 1989; Henderson and McCaig, 1996). This is consistent with widespread calcite mineralization in the breccia and fractures (veins).

Mineral precipitation will seal the fractures, reducing permeability. As a result, fluid pressures eventually may rise again.

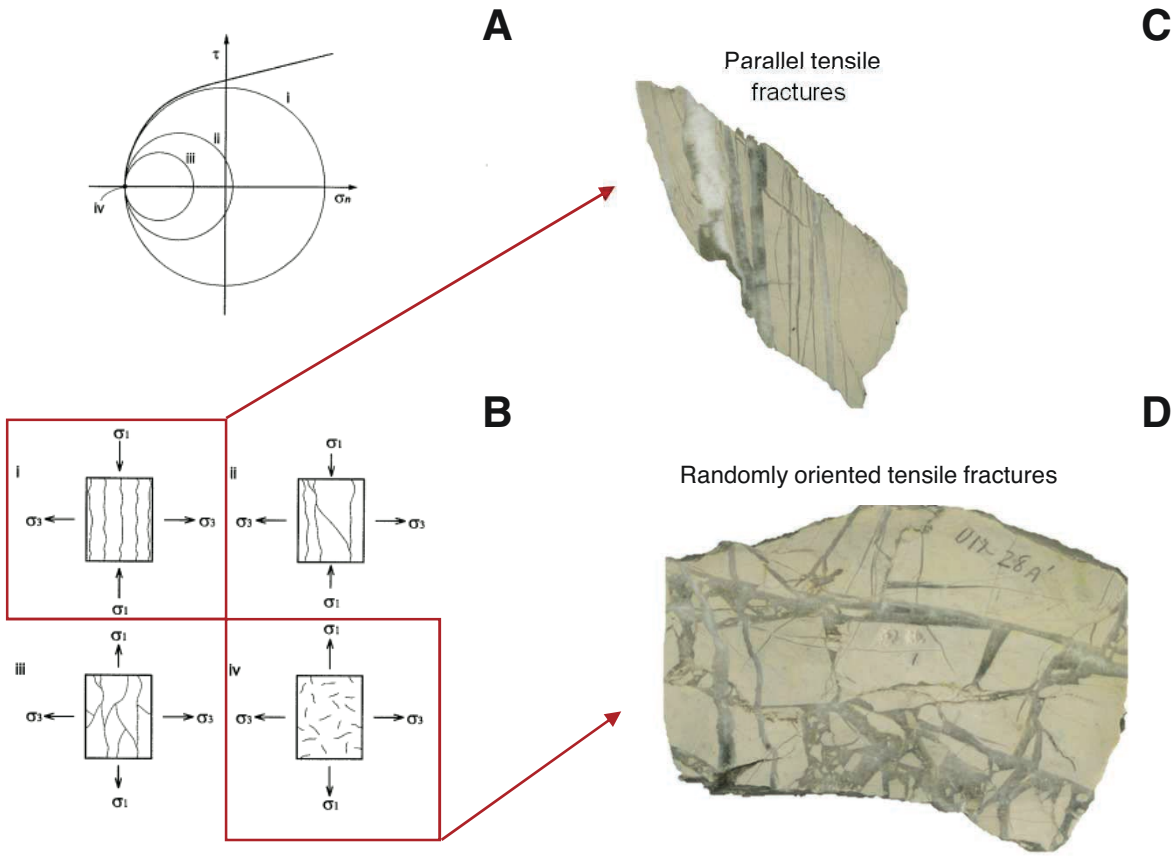

Figure 5. (A) Mohr circles representing a range of stress states that will lead to tensile failure. (B) Patterns of tensile fractures generated, respectively, by the four stress states shown in A (adapted from Cosgrove, 1995; used with permission from the Geological Society of London). (C) A regular array of tensile fractures exposed on a bedding plane at Colle gli Scogli locality. The alignment of the veins indicates that a significant differential stress existed during fracturing. (D) Randomly orientated tension fractures, which indicate a hydrostatic stress state during fracturing (Colle gli Sogli locality).

This cyclical behavior of rising fluid pressure until sudden fracturing, release of fluid, and reduction of fluid pressure is known as "seismic pumping" (Sibson et al., 1975; Nor and Walder, 1992; O'Hara and Haak, 1992), a process that is responsible for creating multiple generations of fracturing and mineralization, which can often be inferred from crosscutting relationships. Such a mechanism applies well to the breccia walls in this study. For instance, at the Gola del Corno and Fonte della Vernosa localities (Monte Catria Walls), we observed two generations of calcite. The first generation consists of calcite veins, which are crosscutting the breccia fragments but terminate at the fragments edges. The second generation of calcite is the calcite fill in between the breccia fragments. For the Colle gli Scogli transect, because of the striking similarity in petrographic textures and isotopic signatures of the calcite in both the calcite veins and breccia, the planar veins seem to be transitional to the breccia, so here we can infer only one generation of calcite.

Origin of High-Pressure Fluids: Constraints from Sr, O, and C Isotope Ratios

The strontium isotopic composition ($^{87}Sr/^{86}Sr$) of calcite can be used as a proxy to determine the source of the fluids depositing the calcite cement in the fractures (veins) and breccia matrices. As Sr^{2+} substitutes for Ca^{2+} during chemical precipitation of marine carbonates and evaporites, the $^{87}Sr/^{86}Sr$ ratio of the precipitate reflects the $^{87}Sr/^{86}Sr$ ratio of the fluid at the time of deposition, assuming no isotopic fractionation has occurred (Faure and Powell, 1972). Furthermore, the $^{87}Sr/^{86}Sr$ value of Sr dissolved in the world's oceans has varied though Phanerozoic time in a known way, allowing the $^{87}Sr/^{86}Sr$ ratio to be used as a stratigraphic tool to date and to correlate marine sedimentary rocks worldwide by comparison with an established seawater Sr reference curve (Burke et al., 1982; Smalley et al., 1994; McArthur et al., 2001, 2012), providing no diagenetic alteration has occurred. While Sr isotopes do not fractionate when incorporated in marine carbonate, oxygen isotopic ratios do. The $\delta^{18}O$ value of the mineralizing calcite is determined by the $\delta^{8}O$ composition of the fluid depositing the calcite (seawater, meteoric water, basinal brines), which is a function of temperature (Shackleton, 1967). Crossplots and mixing diagrams incorporating both strontium and oxygen isotopic ratios are a useful tool for inferring the relative contributions of the different sources ("end members") contributing to the isotopic signature of the calcite deposited from a fluid, and they can therefore provide crucial information about rock-water interaction and fluid migration pathways.

In Figure 6, the seawater Sr reference curve (McArthur et al., 2001) is plotted along with the stratigraphy of the Umbria-Marche sedimentary sequence deposited during the Triassic to Paleocene. When plotted on the seawater reference curve (Fig. 6), the Sr isotope ratios of the breccia fragments in the Maiolica Formation and Scaglia Rossa (host rocks) tie them to a small stratigraphic window. The Maiolica Formation fragments, which exhibit a Sr isotope ratio of ~0.7075, are of Hauterivian–Barremian age. The Scaglia Rossa fragments ($^{87}Sr/^{86}Sr$ ~0.7073–0.7074) in the breccia originate from the R1 member (Montanari and Koeberl, 2000, their figure 4.1.2), the stratigraphic age of which is Turonian–Santonian. The Sr isotope ratios of the calcite veins, and the calcite in breccia fill supporting the brecciated fragments have no age implication, but instead they reflect the signature of the fluid source, or the compositional mixing between an external fluid and the host rock. As the Sr isotope ratios of the calcite veins and matrix are consistently shifted toward higher $^{87}Sr/^{86}Sr$ ratios by 0.0002 (0.7075 for calcite cement in Scaglia Rossa breccia, and 0.7077 for calcite cement in Maiolica Formation breccia, respectively) compared to the host rock (0.7073 and 0.07075 for Scaglia Rossa and Maiolica, respectively), the contribution from a fluid with higher $^{87}Sr/^{86}Sr$ ratio is required to explain this signature, and the fluid must have been buffered to a large extent by the host rock to provide the consistent shift with respect to the host rock. In most localities, except for the Gola del Corno, there is no evidence of dissolution of the breccia fragments. Fine-grained calcite produced by brecciation of the host rock may have provided a large fluid-breccia interface, resulting in cation exchange providing calcium to the solution, and promoting equilibrium with respect to the calcite cementing the breccias.

High $^{87}Sr/^{86}Sr$ ratios may originate from (1) a radiogenic source, such as crustal contamination originating from deep thermometamorphic reactions, (2) marine pore waters with elevated $^{87}Sr/^{86}Sr$ ratio, expelled or recycled from deeper or higher up the stratigraphic column, or (3) fluids that interacted during diagenesis of siliciclastic rocks, such as clay-mineral transformations.

Oxygen and carbon isotope ratios are less consistent with a fluid source originating from (1) evolved meteoric water or (2) hot, deep hydrothermal brines from thermometamorphic reactions. Migration of meteoric groundwater entering the rocks after rise of the anticlines above sea level during the Neogene Apennine orogenesis, followed by reinjection back into the Maiolica Formation along faults, would shift the $\delta^{13}C$ to highly negative values (provided they equilibrated with soil-derived CO_2), which is inconsistent with our observations. For reference, the $\delta^{13}C$ values of infiltrating waters in present-day Apennine and Tuscany carbonate aquifers vary between –18‰ to –28‰ (Collettini et al., 2008). A meteoric source would only be plausible if it were mixed with fluids that did not equilibrate with the soil during infiltration, and if there were substantial mixing with crustal fluids providing elevated Sr and O isotope ratios. Furthermore, Fe and Mn concentrations in the calcite veins and breccia cements are very low. As Fe and Mn are multivalent, they are both sensitive to Eh and pH controls. They occur in very low concentrations in seawater but are present in higher concentrations in groundwater and oil-field brines (Veizer, 1983). The low contents seem to exclude a meteoric origin.

Deep hydrothermal brines would shift the $\delta^{18}O$ to very low values, due to the temperature-dependent oxygen isotope fractionation between calcite and the mineralizing fluid. Furthermore, at the Monte Cucco locality, where there is only one generation

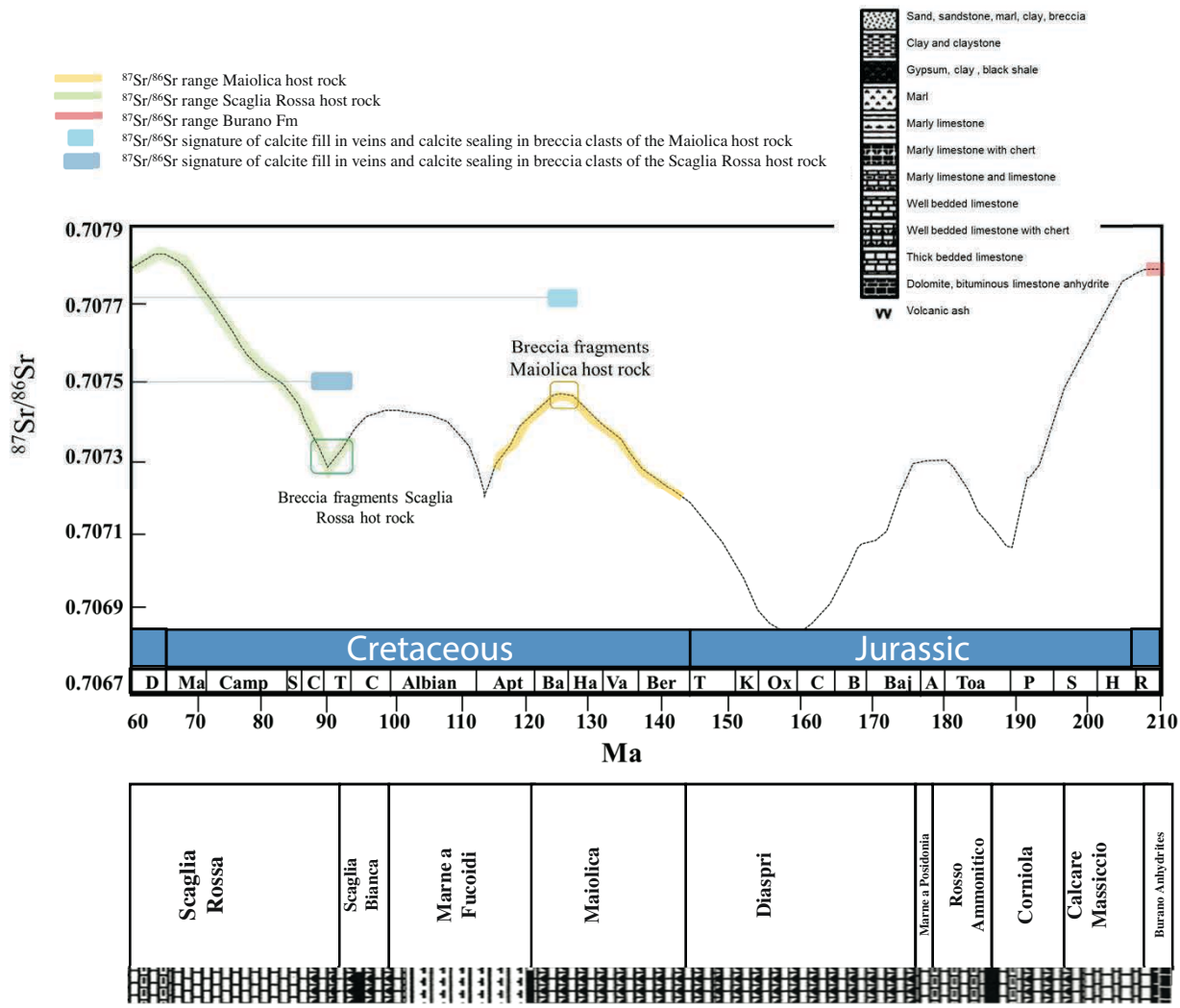

Figure 6. Seawater reference curve for $^{87}Sr/^{86}Sr$ displaying the natural variations of this isotope ratio from the Triassic to Paleocene, as recorded in marine carbonates (modified from McArthur et al., 2001). Plotted are the Sr isotopic ratio of the breccia host rock, defining the stratigraphic window in which the breccias occur (rounded rectangles), and the isotopic composition of the calcite veins and calcite fill supporting the breccia fragments. Also depicted is the Sr isotope ratio of the Burano anhydrites deeper down the stratigraphic column, which may have been a source for the fluids depositing the calcite in the breccia. Please note that the Sr isotopic composition of the calcite veins and calcite fill supporting the breccia has no age implication but reflects the mixing between the host rock and the fluid depositing the calcite. Abbreviations on the geological time scale indicate the different stages during the Paleogene, Cretaceous, and Jurassic. Paleogene: D—Danian. Cretaceous: Ma—Maastrichtian, Camp—Campanian, S—Santonian, C—Coniacian, T—Turonian, C—Cenomanian, Apt—Aptian, Ba—Barremian, Ha—Hauterivian, Va—Valanginian, Ber—Berriasian. Jurassic: T—Tithonian, K—Kimmeridgian, Ox—Oxfordian, C—Callovian, B—Bathonian, Baj—Bajocian, A—Aalenian, Toa—Toarcian, P—Pliensbachian, S—Sinemurian, H—Hettangian. Triassic: R—Rhaetian. Stratigraphy and lithology are from Montanari and Koeberl (2000).

of calcite in the breccias, the oxygen isotope compositions of the calcite veins and calcite in the matrix are positively shifted by 4‰ (from $\delta^{18}O$ ~–2‰ in the Maiolica Formation host rock to +2‰ in the calcite cements). Assuming the fluids depositing the calcite originated from deeper down the stratigraphic column, the only possible candidate source rocks containing a signature with both elevated $^{87}Sr/^{86}Sr$ ratios and positive $\delta^{18}O$ values are the Burano Anhydrite (ca. 210 Ma; see stratigraphy in Fig. 6), which yield a $^{87}Sr/^{87}Sr$ ratio of 0.7080 and a $\delta^{18}O$ of 10.8‰ ± 1.2‰ (Boschetti et al., 2011), or cold fluids expelled from deep thermometamorphic reactions involving a large crustal component, which are known to yield high $^{87}Sr/^{86}Sr$ ratios and $\delta^{18}O$ values. An overview of Sr, O, and C isotopic signatures of breccia host clasts, veins, and calcite breccia fills is provided in Figure 7, along with possible fluid sources depositing the sparry calcite in the breccia fills and veins.

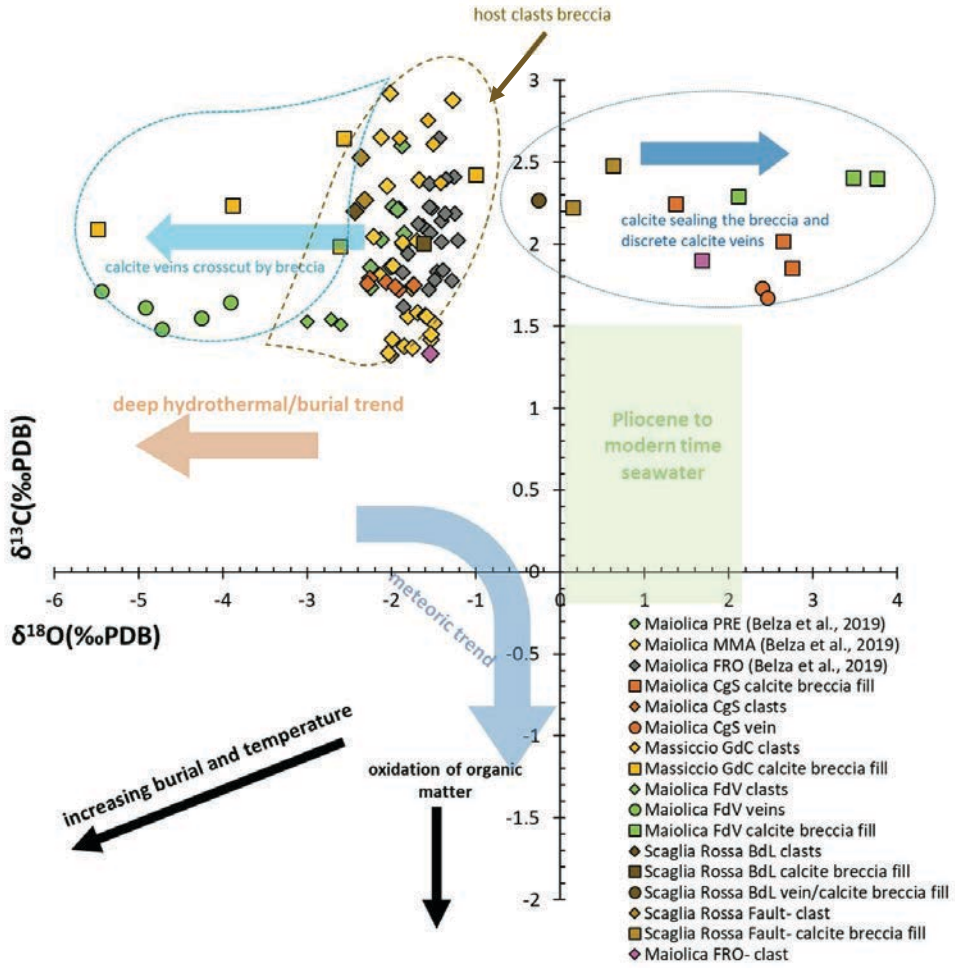

Figure 7. $\delta^{18}O$ vs. $\delta^{13}C$ cross-plot for calcite veins, breccia calcite fill, and breccia host clasts. Along the Monte Cucco breccia wall exposures, there is only one generation of calcite, which is present as discrete calcite veins east of the solution tectonite along the Colle gli Scogli transect and as calcite fill sealing the breccia Maiolica clasts in the expansion breccia westward of the solution tectonite. There are two generations of calcite in the Fonte della Vernosa and Gola del Corno localities (Monte Catria breccia wall exposure): the first generation, calcite veins, is shifted toward negative $\delta^{18}O$ values, while the breccia calcite fill exhibits the same $\delta^{18}O$ signature as the Monte Cucco wall exposures, suggesting a common source of the fluids depositing the calcite fill in the breccia in all breccia wall exposures. Elevated $\delta^{18}O$ in the breccia calcite fill is inconsistent with deep hydrothermal fluids or meteoric infiltration, as these would have shifted the oxygen or carbon isotopic signature to very low values (deep hydrothermal trend and meteoric trend, respectively). The temperature-dependent fractionation between water and calcite, shifting calcite deposited from hot fluids to very low $\delta^{18}O$ values, requires the fluids to be relatively cold during calcite mineralization, so these are not hydrothermal breccias. See Figure 3 for locality abbreviations. PDB—Peedee belemnite; PRE —Presale locality; MMA—Monte Acuto locality.

Burano Anhydrites

In the Triassic, sedimentation in the Apennines Umbria-Marche region began with the deposition of an evaporite sequence known as the Burano Anhydrite (Anidriti di Burano; Martinis and Pieri, 1964). The Upper Triassic Burano Anhydrite is a 2–2.5-km-thick sequence composed of meter- to decameter-scale alternating gypsum-anhydrite beds and dolostones. Anhydrites were originally deposited as gypsum in a shallow-water environment (Ciarapica and Passeri, 1976; Lugli, 2001). During burial, the gypsum layers became dehydrated to anhydrite.

Gypsum ($CaSO_4 \cdot 2H_2O$) is a hydrated mineral that contains 20.9% crystallization water by weight. The $\delta^{18}O$ value of the hydration water records the isotope ratio of the mother water from which the gypsum crystallized. Provided the fractionation factors are known and no isotopic exchange has occurred after crystallization, the $\delta^{18}O$ value of the water can be used to calculate the $\delta^{18}O$ of the gypsum hydration water. In evaporitic environments, the equilibrium isotopic fractionation between gypsum and mother brine (Kasprzyk and Jasińska, 1998) can be described as

$$\alpha = \frac{1000+\delta gypsum}{1000+\delta brine}, \quad (2)$$

with the fractionation factor α determined to be 1.004 (Gonfiantini and Fontes, 1963). In addition, the isotopic composition of the crystallization (hydration) water of gypsum is enriched by 4‰ in oxygen relative to the isotope ratios of mother solutions (Gonfiantini and Fontes, 1963). Boschetti et al. (2011) measured $\delta^{18}O$ in Burano Formation anhydrite deposits, yielding $\delta^{18}O$ values of 10.8‰ ± 1.2‰ (expressed against Vienna standard mean ocean water [VSMOW], the standard against which isotopic compositions of both hydrogen and oxygen are reported). Applying the equilibrium fractionation equation outlined above, and the 4‰ positive shift in the hydration water compared to the mother brine, the corresponding $\delta^{18}O$ of the gypsum crystallization (hydration) water is estimated to be 14‰–15‰.

Furthermore, during burial and dehydration of the gypsum to anhydrite, a considerable mass of water is removed, and most of the Sr is mobilized within this dehydration water. If this

formation water were the source of the fluids depositing the calcite cement in the breccia matrix, the Sr concentrations should be much higher than our results. Anhydrites contain significant amount of Sr, up to several 1000 ppm, and would increase the Sr concentration of the calcite deposition fluid. On the contrary, the Sr concentrations in the calcite deposited in the veins and breccia matrix are rather low, yielding similar concentrations as the breccia host rock (100–200 μg g^{-1} for Maiolica Formation, 200–400 μg g^{-1} for Scaglia Rossa Formation). Furthermore, during dehydration, the escaping water is saturated with respect to $CaSO_4$ and can create sparry anhydrite cements in adjacent nonevaporite cements. This is in strong contradiction to our observations, which yield only $CaCO_3$ cements.

Although the kinetics of the gypsum dehydration reaction are poorly understood and prevent assessment of the exact timing of the onset of the dehydration reaction, De Paola et al. (2008) estimated that conditions for the dehydration reaction should be satisfied within the entire volume of Triassic evaporites when the overlying Calcare Massiccio Formation reached a critical thickness of 700 m (during the Hettangian–Sinemurian). The dehydration process was probably completed by the Late Cretaceous–Early Tertiary, when more than 2 km of pelagic carbonate rocks had been deposited on top of the evaporites (De Paola et al., 2008). During the Paleogene, the Triassic evaporites became involved in the Apennine orogeny. The large time gap between dehydration and calcite cementation (for which the inferred stratigraphic framework is the Pliocene–present time, with the onset of extension) in the breccias makes the anhydrites from the Burano Formation a less likely source for the fluids involved in the hydraulic fracturing (brecciation) and sealing of the breccia walls.

Clay-Mineral Reactions

The conversion of smectite to illite or chlorite is accompanied by the release of a large quantity of both interlayer and structural water. This dehydration process may lead to overpressure and variable pressure regimes (Burst, 1969; Bruce, 1984; Lynch, 1997). Chloritization may also lead to release of calcium (and possibly magnesium) and thus may lead to minor carbonate cementation, but only if bicarbonate is present in the formation water or CO_2 is present in a gas phase (McKinley et al., 2013).

However, dehydration during conversion of smectite to illite is unlikely to provide the amount of CO_2 necessary to generate explosive fragmentation, producing the breccias, unless production of hydrocarbons was also involved. If this was the case, this would have led to a significant decrease in the $\delta^{13}C$ values of the fluids and the calcite deposited, which is in strong contradiction to our analyses. Furthermore, this process also does not explain the widespread calcite mineralization in the breccias and vein, as fluids released during conversion of smectite to illite are not able to provide Ca-saturated fluids. According to the chemical formula of typical smectite ($[Ca_{1/2},Na]_{0.35}[Al,Mg]_2Si_4O_{10}[OH]_2 \cdot nH_2O$) and illite ($[K,H_3O]Al_2Si_3AlO_{10}[OH]_2$), the transformation of smectite to illite is accompanied by the release of aqueous silica, Mg^{2+}, and water (Roland and Ola, 1996), frequently resulting in concomitant quartz cementation (Chen et al., 2013). Neither an increase in Mg content in the calcite cementing the breccias nor quartz cementation is observed in the studied breccia samples. Clay-mineral transformation is therefore not considered to have taken part in the formation of these breccias.

Crustal Source of Fluids?

Constraints from $^{87}Sr/^{86}Sr$ and $\delta^{18}O$. As suggested by $^{87}Sr/^{86}Sr$ and $\delta^{18}O$ isotopic data for the calcite veins and breccia matrix, other possible sources of generation of fluid overpressure required for hydraulic fracturing and cementation of the breccia walls are fluids expelled from deep thermometamorphic reactions involving a large crustal component, which are known to yield high $^{87}Sr/^{86}Sr$ and $\delta^{18}O$ isotope ratios. Thermometamorphic reactions involving silicate and carbonate, such as decarbonation reactions, are known to release a significant amount of CO_2. In the Umbria-Marche Apennines, CO_2 overpressures have been recorded in two deep (4–5 km) boreholes (e.g., San Donato and Santo Stefano) within the Triassic Burano evaporites. These observed CO_2 overpressures occur within dolostones that are sealed by Ca-sulfate (anhydrite) horizons (Collettini et al., 2008), suggesting that stratigraphic seals (e.g., the Triassic evaporites) can act as traps for the CO_2-rich fluids and promote the development of fluid overpressures (Collettini et al., 2008).

However, carbon isotopic data, CO_2 fugacity, and temperatures and pressures are not compatible with typical thermometamorphic or hydrothermal reactions (Marini and Chiodini, 1994; Chiodini et al., 2000; Collettini et al., 2008). Collettini et al. (2008) argued that given the low heat flux in the Central Apennines (with a normal geothermal gradient of ~30 °C/km), thermometamorphic temperatures can occur in the natural environment only at depths in the range of 11–17 km, which is consistent with lithostatic pressures of 3–4.5 kbar, i.e., well above that in equilibrium for CO_2 generation. Instead, carbon and helium isotopic data suggest the source of the deep-seated CO_2 in central Italy is mantle-derived, such as crustal fluids derived from the subducting Adriatic plate metasomatizing the overlying mantle wedge (Chiodini et al., 2000, 2004; Collettini et al., 2008; Frezotti et al., 2009). Solid carbonates, comprising a large component of the subducting Adriatic crust, may have formed carbonate-rich (hydrous silicate) melts (Frezotti et al., 2009) at pressures >4 GPa, which, due to their low density and viscosity, migrated upward through the mantle, forming a carbonated, partially molten, CO_2-rich mantle layer. Upwelling of these melts to lower depths would have induced massive outgassing of CO_2 (Frezotti et al., 2009), which could then be tapped from the metasomatized upper mantle into in the lower crust by a set of major east-dipping normal faults, which in the Apennines are known to accommodate extension within the brittle upper crust (Barchi et al., 1998). This is consistent with the conceptual model of Chiodini et al. (2004) and Collettini et al. (2008), which explains subaerial degassing of deep-seated CO_2 in the western part of central Italy (Tuscany, Latium), and its contrasting absence in the active

seismic area of the Umbria-Marche region, where CO_2 is only present in deep-seated, structural traps, creating overpressures and promoting earthquake nucleation.

Hydrofracturing in response to overpressure of such a CO_2-rich fluid is a likely scenario for the formation of these breccias. The Apennines have been affected by deep-seated CO_2 degassing since the onset of extension in the middle Pliocene (Chiodini et al., 2004). Oversaturation of CO_2 under confining pressure in deep reservoirs or a sudden decompression of the CO_2-saturated water could lead to rapid exsolution of the dissolved gas. Large volume expansion of the bubbly liquid and high buoyancy could cause rapid upward acceleration, resulting in fracturing (Uysal et al., 2009).

During CO_2 degassing from aqueous solutions, kinetic isotopic fractionations occur that will affect the isotopic compositions of both the degassed CO_2 and the carbonate minerals that precipitate from the partially degassed fluids (Guo et al., 2009) according to the reaction:

$$Ca^{2+} + 2HCO_3^- \leftrightarrow CaCO_3\downarrow + CO_2\uparrow + H_2O. \quad (3)$$

Based on model predictions, Guo (2009) found that isotopic fractionations during CO_2 degassing from aqueous solutions increase the $\delta^{13}C$ and $\delta^{18}O$ values of the residual dissolved inorganic carbon (DIC) species and of the carbonate minerals that precipitate from the DIC pool. Moreover, as calcite precipitates, residual waters become enriched in ^{18}O, thus driving the $\delta^{18}O$ of later-formed calcite to higher values. This would explain the positive $\delta^{18}O$ values in the calcite cementing the breccias, and the slight enrichment in $\delta^{13}C$. This disequilibrium mineralization, caused by kinetic isotopic fractionation, has also been described in modern speleothem calcite (figure 6 *in* Mickler et al., 2004).

Furthermore, Guo et al. (2009) stated that a fluid containing Ca^{2+} and DIC that undergoes degassing of CO_2 will be subjected to an increase in pH, promoting precipitation of $CaCO_3$. This is consistent with the widespread calcite mineralization within the breccia matrix.

Assuming that crustal fluids derived from the subducting Adriatic plate and involved in metasomatization of the overlying mantle wedge are the source of the CO_2, we can explain the Sr, C, and O isotopic signatures of the calcite cementing the Maiolica Formation and Scaglia breccias. Turi and Taylor (1976) and Holm and Munksgaard (1982) measured Sr and O isotope ratios of volcanic rocks (Vulsinian District, central Italy) formed from little-modified mantle-derived magmas. These magmas are high in both radiogenic Sr ($^{87}Sr/^{86}Sr$ = 0.7103–0.7107) and $\delta^{18}O$ (11.2‰–16.4‰ VSMOW) and were interpreted to have been inherited from a metasomatized parental mantle, in which hydrous fluids enriched in large ion lithophile elements (Sr, Rb) and high in $\delta^{18}O$ and $^{87}Sr/^{86}Sr$ would have mixed with mantle of "normal," lower $\delta^{18}O$ and $^{87}Sr/^{86}Sr$. These studies attributed the origin of the fluids to dehydration of continent-derived sediments that were subducted beneath a mantle wedge during subduction of the Adriatic plate beneath the Corsica-Sardinia block.

The $\delta^{13}C$ values of the calcite in the breccia matrix and discrete calcite veins are slightly elevated compared to the host rock. If the CO_2-rich fluid driving fragmentation and formation of the breccias and causing calcite mineralization was derived from a metasomatized mantle, the carbon isotopic signature should be inherited in the calcite. According to Collettini et al. (2008), the current $\delta^{13}C$ isotopic composition of deeply derived CO_2 in the Central Apennines is in the range of –5 to +1.5‰. Furthermore, the $\delta^{13}C$ of CO_2 released at Italian volcanoes is around 0.06‰–0.034‰ (Mason et al., 2017). Such elevated $\delta^{13}C$ values have been linked to a high degree of crustal carbonate contamination in the mantle (Mason et al., 2017). Although these values are lower than the $\delta^{13}C$ of the calcite matrix and discrete calcite veins in this study, the $\delta^{13}C$ of the fluids would be shifted toward higher values during CO_2 degassing. An overview with $\delta^{13}C$ values of proposed fluid sources versus calcite in breccia matrix and discrete veins is depicted in Figure 8.

Cyclic pressure buildup. The presence of two generations of calcite in the breccias and their observed difference in degree of fracturing (parallel veins crosscutting angular clasts of expansion breccias) reflect the evolution in stress and fluid pressure state and attest to gradual, cyclic pressure buildup and release. The first fracturing event produced extension fractures, providing a permeability pathway for deep, mantle-derived CO_2-rich fluids and depositing sparry calcite, sealing the pathway, and further increasing the pressure. The second hydrofracturing event was produced during a sudden release of a highly overpressured, CO_2-rich fluid, resulting in expansive fragmentation and formation of the breccias.

This is particularly evident from the breccias at Gola del Corno and Fonte della Vernosa (Monte Catria wall). Isotopic data are consistent with this scenario of a polyphase fluid regime: At the Gola del Corno and Fonte delle Vernosa localities, where there are several generations of calcite, the first generation of calcite has contrasting lower $\delta^{18}O$ values but similar $^{87}Sr/^{86}Sr$ values and slightly lower $\delta^{13}C$ values compared to the calcite breccia fill, representing the second fracturing event. If the fluids had the same origin, the difference in the $\delta^{18}O$ could be explained by a different mineralizing temperature of the calcite, while the slight decrease in $\delta^{13}C$ may relate to a lower degree of CO_2 degassing. Contrary to $\delta^{13}C$ and $^{87}Sr/^{86}Sr$, $\delta^{18}O$ is the only system that is temperature-dependent. Higher temperatures, to be expected during temperature- and pressure-driven flow of deep-seated fluids during the first fracturing event, would increase the $\delta^{18}O$ value of the calcite deposited in the veins but leave the $\delta^{13}C$ and $^{87}Sr/^{86}Sr$ unaltered. The second fracturing event, driven by rapid CO_2 degassing, would cause a rapid drop in temperature and pressure, increasing the $\delta^{18}O$ and $\delta^{13}C$ values of the fluids depositing the calcite in the breccia matrix.

Evidence of CO_2 degassing related to calcite precipitation is found in the widespread presence of subaerial travertine deposits in the Central Apennines (Hancock et al., 1999; Uysal et al., 2009). In the Apennines, travertine deposits occur along active extensional faults (Ascione et al., 2014). Travertine is formed

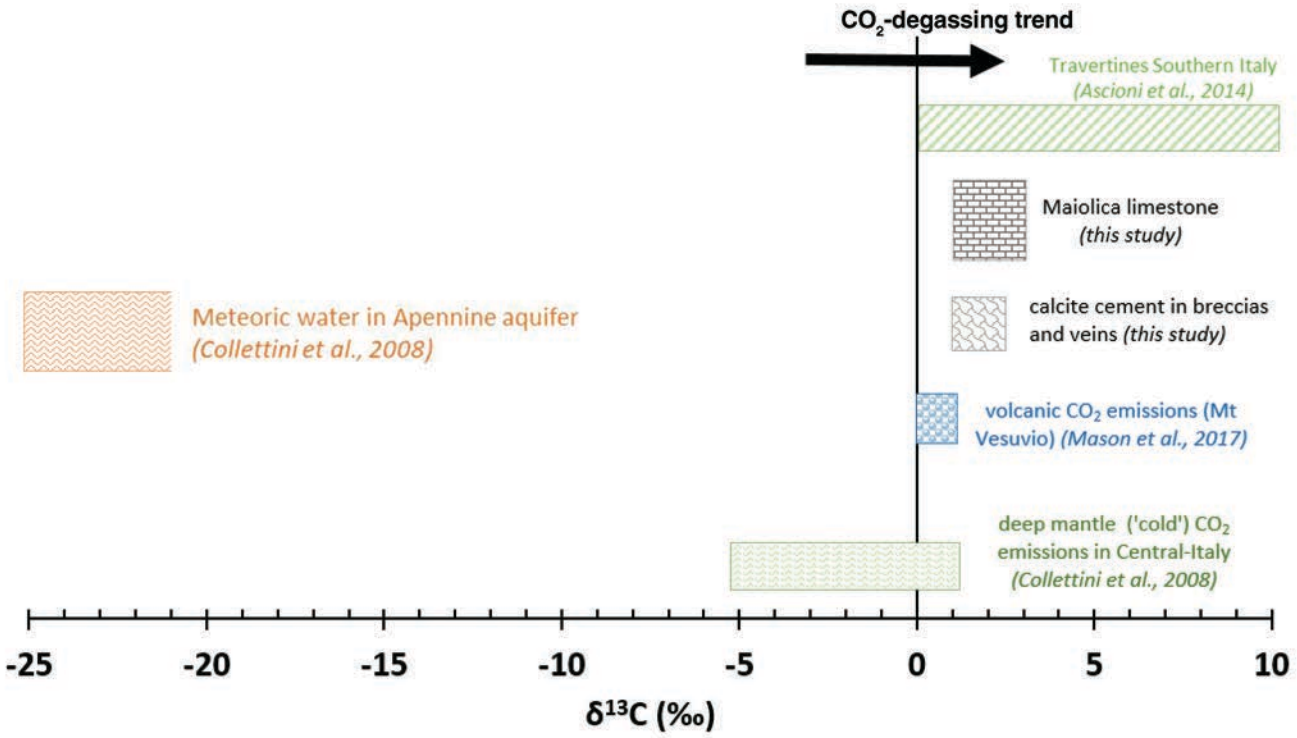

Figure 8. Diagram showing $\delta^{13}C$ values of proposed fluid sources versus calcite breccia fill and discrete veins. Meteoric fluids would shift the carbon isotopic signature to lower $\delta^{13}C$ values (provided they interacted with soil CO_2 during infiltration), which is inconsistent with our observations in the calcite cementing the breccia and veins. The $\delta^{13}C$ value for CO_2 from a metasomatized mantle is slightly lower than the $\delta^{13}C$ in the calcite cements, but it would shift to higher $\delta^{13}C$ during CO_2 degassing, as is proposed to be the driving mechanism for brecciation.

by carbonate deposition in a thermal spring system, providing hypersaturated alkaline-sulfate waters resulting from a deep hydrothermal circulation into carbonate/sulfate-rich bedrock. When the fluids reach the surface, they will degas as a result of lower atmospheric pCO_2, resulting in an increase in pH. As the solubility of calcium carbonate decreases with increased with pH, calcite is precipitated. The geothermal affinity of the waters depositing the travertine limestone in the Central Apennines is substantiated by their characteristic positive values of $\delta^{13}C$, supporting the recycled, marine/evaporitic provenance of carbon unrelated to the meteoric/biochemical activity of vegetation and soils (Gandin and Capezzuoli, 2008, 2014).

An interesting aspect of this scenario is that the widespread calcite mineralization, its geochemical signature, and the absence of gypsum or Mg-rich calcite cements suggest the CO_2-rich fluids seemingly did not interact with the evaporite seals.

The solubility of gypsum in pure water is roughly four orders of magnitude greater than the solubility of $CaCO_3$. Gypsum solubility under pressure conditions relevant for CO_2 geological storage has been investigated by Rendel et al. (2016). Although the dissolution of calcite is enhanced in the presence of CO_2, the gypsum solubility is decreased (Rendel et al., 2016). If the CO_2-rich fluids interacted with limestone/dolostone/evaporites, they were saturated with respect to calcium carbonate. In order to further constrain this, we are planning analyses of fluid inclusions in the near future.

Constraints from Petrographic Textures, CL, and Mn and Fe Contents

As emphasized in our companion paper (Alvarez et al., this volume), it may be significant that most of the fill calcite is blocky, rather than elongate fibrous or fibrous (Bons et al., 2012, their figure 14). Blocky fill is indicative of high strain rates during crack opening and the presence of fluids with sufficiently high fluid pressure to keep the crack open throughout the crystallization history (Van der Pluijm and Marshak, 2004, p. 160). This is important because the breccia fragments would otherwise not have been able to remain separated while the calcite was deposited.

Another interesting aspect is that there is little mechanical calcite twinning in the coarse fill calcite. Calcite twinning occurs at low values of deviatoric stress, probably <7 MPa, with pressure solution occurring under deviatoric stress that is even less than that required for calcite twinning (Groshong, 1975). These observations support the presence of a carbonate-rich fluid under a high enough fluid pressure for a sufficiently long time interval to form the "blocky" texture, with no subsequent

compressive stresses sufficiently high to cause twinning (Alvarez et al., this volume).

Furthermore, the faint discontinuous zoning and rather homogeneous CL color suggest very rapid crystallization from a rather homogeneous source. The discontinuous zoning, which appears as a stacking of arrowhead to triangular blocks, appears rather similar to the so-called fir-tree zoning (Raven and Dickson, 1989). This fir-tree zoning, which appears as triangular blocks, arrowhead blocks, and fir-tree arrays, has been previously described in calcite filling fissures, and it is hypothesized to be an indicator of pulsed crystallization in calcite cement crystals. Raven and Dickson (1989) stated that the zoning is caused by a combination of sector zoning and abrupt changes in relative growth rate of adjacent sectors. The ubiquitous presence of this texture in the calcite fill would indicate the calcite underwent a "pulsed crystallization" process.

This three-dimensional expansion of the breccia fragments, which fit in a jigsaw puzzle, and the lack of repeated crack-and-seal textures in the calcite fill require a single rapid expansion/explosion event for each generation of calcite (veins and breccia fills crosscutting the veins). However, rapid CO_2 degassing would lead to a quick dissipation of the pressure, which may have remained insufficiently high to sustain the fluid flow and the subsequent crystallization of the calcite. The pulsed crystallization may therefore be consistent with pulsed release of CO_2-rich fluids from an overpressured deep reservoir, sustaining the high fluid-flow rates. Alternatively, high-pressure fluid circulation may have been enhanced by the sealing capacity of the overlying impermeable Marne a Fucoidi Formation (Fucoid marls), which was not affected by brecciation.

Understanding the role of CO_2 overpressure and its relation to expansion events is important in assessing the current seismic hazard in the central part of the Umbria-Marche Apennines, where the strongest historical earthquakes are located (Boschi et al., 2000). In the active area of the Northern Apennines, both along the Altotiberina low-angle normal fault and in the hanging-wall rocks, very small repeating earthquakes have been documented (Chiaraluce et al., 2007). These repeating earthquakes occur in very small slip patches with dimensions on the order of 10–100 m and within a very short time delay from each other (i.e., minutes/hours). The breccias described in this manuscript may represent an ancient exhumed analogue for these repeating earthquakes.

CONCLUSION

(1) At several places in the anticlinal structures forming the Apennine fold-and-thrust belt, the Maiolica and Scaglia Rossa Formations are affected by the presence of hydraulically fractured calcite-cemented breccias (expansion breccias) and calcite veins.

(2) Both breccias and veins are an expression of hydraulic fracturing and acted as permeability pathways, allowing the deposition of sparry calcite with elevated $^{87}Sr/^{86}Sr$ and positive $\delta^{18}O$ values. This calcite was deposited and filled the veins once the excess of fluid pressure had dissipated.

(3) Strontium and oxygen isotope ratios in the breccia-sealing calcite cement are consistent with a source of deep-seated, CO_2-rich fluids such as crustal fluids derived from the subducting Adriatic plate metasomatizing the overlying mantle wedge (Chiodini et al., 2004; Collettini et al., 2008). These fluids interacted with and may have led to the dissolution carbonates in the Umbria-Marche pelagic succession, loading the CO_2-rich fluids with Ca. Those fluids would have been trapped by structural or stratigraphic seals (anhydrites, dolostones), overpressurizing the system and resulting in brecciation. This hypothesis is consistent with the conceptual model of Chiodini et al. (2004) and Collettini et al. (2008).

(4) As such, the geochemical signatures of the calcite deposited in the extensional, parallel fractures, and the calcite cementing the expansion breccias reflect the signature of a mantle-derived CO_2 fluid, as well as interaction with their stratigraphic seal (Burano Anhydrites/dolomites/limestones), and the Maiolica and Scaglia Rossa host rocks.

(5) There are at least two generations of calcite in the breccias at Gola del Corno and Fonta delle Vernosa (Monte Catria breccias). The first generation consists of the calcite veins, which exhibit elevated $^{87}Sr/^{86}Sr$ ratios and negative $\delta^{18}O$ values. The second generation is the sparry calcite cementing the breccia, which yields elevated $^{87}Sr/^{86}Sr$ and positive $\delta^{18}O$ values, similar to the signature in the calcite sealing the Monte Cucco breccia walls, suggesting they belong to the same hydrofracturing event.

(6) The presence of two generations of calcite in the breccias and their observed difference in degree of fracturing (parallel veins crosscutting angular clasts of explosion breccias) reflect the evolution in the stress and fluid pressure state and attest to gradual, cyclic pressure buildup and release. The first hydrofracturing event produced extension fractures, providing a permeability pathway for deep, CO_2-rich fluids to deposit sparry calcite. The second hydrofracturing event was produced during a sudden release of a highly overpressured, CO_2-rich fluid, resulting in expansive fragmentation and formation of the breccias. A peculiar growth texture ("fir-tree zoning") revealed by CL in calcite crystals from the breccia matrix could indicate pulsed crystallization under abrupt pressure changes.

ACKNOWLEDGMENTS

Joke Belza acknowledges the Research Foundation Flanders (FWO) for its support in funding a Ph.D. fellowship. Alessandro Montanari and the Geological Observatory of Coldigioco provided logistical support during fieldwork. We would like to acknowledge the editor and reviewers for careful reading and

constructive suggestions that substantially improved the quality of this manuscript.

REFERENCES CITED

Alvarez, W., 1989a, Evolution of the Monte Nerone seamount in the Umbria-Marche Apennines: 1. Jurassic–Tertiary stratigraphy: Società Geologica Italiana Bollettino, v. 108, p. 3–21.

Alvarez, W., 1989b, Evolution of the Monte Nerone seamount in the Umbria-Marche Apennines: 2. Tectonic control of the seamount-basin transition: Società Geologica Italiana Bollettino, v. 108, p. 23–29.

Alvarez, W., 2009, The historical record in the Scaglia limestone at Gubbio: Magnetic reversals and the Cretaceous-Tertiary mass extinction: Sedimentology, v. 56, no. 1, p. 137–148, https://doi.org/10.1111/j.1365-3091.2008.01010.x.

Alvarez, W., Belza, J., Chan, L.S., Claeys, P., Geiser, P., Menichetti, M., Shimabukuro, D.H., and Tavarnelli, E., 2019, this volume, Expansion breccias in Lower Cretaceous Apennine pelagic limestones: I. Geological observations, *in* Koeberl, C., and Bice, D.M., eds., 250 Million Years of Earth History in Central Italy: Celebrating 25 Years of the Geological Observatory of Coldigioco: Geological Society of America Special Paper 542, https://doi.org/10.1130/2019.2542(12).

Ascione, A., Iannace, A., Imbriale, P., Santangelo, N., and Santo, A., 2014, Tufa and travertines of southern Italy: Deep-seated, fault-related CO_2 as the key control in precipitation: Terra Nova, v. 26, no. 1, p. 1–13, https://doi.org/10.1111/ter.12059.

Barchi, M., Minelli, G., and Pialli, G., 1998, The crop 03 profile: A synthesis of results on deep structures of the Northern Apennines: Memorie della Società Geologica Italiana, v. 52, p. 383–400.

Barchi, M., Landuzzi, A., Minelli, G., and Pialli, G., 2001, Outer Northern Apennines, *in* Vai, G.B., and Martini, I.P., eds., Anatomy of an Orogen: The Apennines and Adjacent Mediterranean Basins: Dordrecht, Netherlands, Springer, p. 215–253, https://doi.org/10.1007/978-94-015-9829-3_15.

Belza, J., Alvarez, W., Vanhaecke, F., and Claeys, P., 2019, this volume, $^{87}Sr/^{86}Sr$ record from the Lower Cretaceous pelagic Maiolica limestone (Central Apennines, Italy) and its offset from the global seawater reference curve, *in* Koeberl, C., and Bice, D.M., eds., 250 Million Years of Earth History in Central Italy: Celebrating 25 Years of the Geological Observatory of Coldigioco: Geological Society of America Special Paper 542, https://doi.org/10.1130/2019.2542(05).

Bons, P.D., Elburg, M.A., and Gomez-Rivas, E., 2012, A review of the formation of tectonic veins and their microstructures: Journal of Structural Geology, v. 43, p. 33–62, https://doi.org/10.1016/j.jsg.2012.07.005.

Boschetti, T., Cortecchi, G., Toscani, L., and Iacumin, P., 2011, Sulfur and oxygen isotope compositions of Upper Triassic sulfates from Northern Apennines (Italy): Paleogeographic and hydrogeochemical implications: Geologica Acta, v. 9, no. 2, p. 129–147.

Boschi, E., Guidoboni, E., Ferrari, G., Mariotti, D., Valensise, G., and Gasperini, P., 2000, Catalogue of strong Italian earthquakes from 461 B.C. to 1980: Annali di Geofisica, v. 43, p. 609–868.

Bruce, C.H., 1984, Smectite dehydration—Its relation to structural development and hydrocarbon accumulation in the northern Gulf of Mexico basin: American Association of Petroleum Geologists Bulletin, v. 68, p. 673–683.

Burke, W.H., Denison, R.E., Hetherington, E.A., Koepnick, R.B., Nelson, H.F., and Otto, J.B., 1982, Variation of seawater $^{87}Sr/^{86}Sr$ throughout Phanerozoic time: Geology, v. 10, no. 10, p. 516–519, https://doi.org/10.1130/0091-7613(1982)10<516:VOSSTP>2.0.CO;2.

Burkhard, M., 1993, Calcite twins, their geometry, appearance and significance as stress-strain markers and indicators of tectonic regime: A review: Journal of Structural Geology, v. 15, no. 3–5, p. 351–368, https://doi.org/10.1016/0191-8141(93)90132-T.

Burst, J.F.J., 1969, Diagenesis of Gulf Coast clayey sediments and its possible relation to petroleum migration: American Association of Petroleum Geologists Bulletin, v. 53, p. 73–93.

Chen, J., Yang, X., Ma, S., and Spiers, C.J., 2013, Mass removal and clay mineral dehydration/rehydration in carbonate-rich surface exposures of the 2008 Wenchuan earthquake fault: Geochemical evidence and implications for fault zone evolution and coseismic slip: Journal of Geophysical Research–Solid Earth, v. 118, no. 2, p. 474–496, https://doi.org/10.1002/jgrb.50089.

Chiaraluce, L., Chiarabba, C., Collettini, C., Piccinini, D., and Cocco, M., 2007, Architecture and mechanics of an active low-angle normal fault: Alto Tiberina fault, Northern Apennines, Italy: Journal of Geophysical Research–Solid Earth, v. 112, no. B10, B10310, https://doi.org/10.1029/2007JB005015.

Chiodini, G., Frondini, F., Cardellini, C., Parello, F., and Peruzzi, L., 2000, Rate of diffuse carbon dioxide Earth degassing estimated from carbon balance of regional aquifers: The case of Central Apennines, Italy: Journal of Geophysical Research–Solid Earth, v. 105, no. B4, p. 8423–8434, https://doi.org/10.1029/1999JB900355.

Chiodini, G., Cardellini, C., Amato, A., Boschi, E., Caliro, S., Frondini, F., and Ventura, G., 2004, Carbon dioxide Earth degassing and seismogenesis in central and southern Italy: Geophysical Research Letters, v. 31, no. 7, L07615, https://doi.org/10.1029/2004GL019480.

Ciarapica, G., and Passeri, L., 1976, Deformazione da fluidificazione ed evoluzione diagenetica della formazione evaporitica di Burano: Bollettino della Società Geologica Italiana, v. 95, p. 1175–1199.

Collettini, C., Cardellini, C., Chiodini, G., De Paola, N., Holdsworth, R.E., and Smith, S.A.F., 2008, Fault weakening due to CO_2 degassing in the Northern Apennines: Short- and long-term processes, *in* Wibberley, C.A.J., Kurz, W., Imber, J., and Holdsworth, R.E., eds., The Internal Structure of Fault Zones: Implications for Mechanical and Fluid-Flow Properties: Geological Society, London, Special Publication 299, p. 175–194, https://doi.org/10.1144/SP299.11.

Cosgrove, J.W., 1995, The expression of hydraulic fracturing in rocks and sediments, *in* Ameen, M.S., ed., Fractography: Fracture Topography as a Tool in Fracture Mechanics and Stress Analysis: Geological Society, London, Special Publication 92, p. 187–196.

Cresta, S., Monechi, S., Parisi, G., Baldanza, A., and Reale, V., 1989, Stratigrafia del Mesozoico e Cenozoico nell'area Umbro-Marchigiana (Mesozoic–Cenozoic Stratigraphy in the Umbria-Marche Area): Memorie Descrittive della Carta Geologica d'Italia 39, 185 p. [in Italian and English].

De Muynck, D., Huelga-Suarez, G., Van Heghe, L., Degryse, P., and Vanhaecke, F., 2009, Systematic evaluation of a strontium-specific extraction chromatographic resin for obtaining a purified Sr fraction with quantitative recovery from complex and Ca-rich matrices: Journal of Analytical Atomic Spectrometry, v. 24, no. 11, p. 1498–1510, https://doi.org/10.1039/b908645e.

De Paola, N., Collettini, C., Faulkner, D.R., and Trippetta, F., 2008, Fault zone architecture and deformation processes within evaporitic rocks in the upper crust: Tectonics, v. 27, no. 4, 21, https://doi.org/10.1029/2007TC002230.

Eisenlohr, B.N., Groves, D., and Partington, G.A., 1989, Crustal-scale shear zones and their significance to Archaean gold mineralization in Western Australia: Mineralium Deposita, v. 24, p. 1–8, https://doi.org/10.1007/BF00206714.

Faure, G., and Powell, J.L., 1972, Strontium Isotope Geology: New York, Springer-Verlag, 188 p.

Frezzotti, M., Peccerillo, L., Panza, A., and May, G., 2009, Carbonate metasomatism and CO_2 lithosphere-asthenosphere degassing beneath the Western Mediterranean: An integrated model arising from petrological and geophysical data: Chemical Geology, v. 262, no. 1–2, p. 108–120.

Gandin, A., and Capezzuoli, E., 2008, Travertine versus calcareous tufa: Distinctive petrologic features and stable isotope signatures: Italian Journal of Quaternary Sciences, v. 21, no. 1B, p. 125–136.

Gandin, A., and Capezzuoli, E., 2014, Travertine: Distinctive depositional fabrics of carbonates from thermal spring systems: Sedimentology, v. 61, no. 1, p. 264–290, https://doi.org/10.1111/sed.12087.

Gonfiantini, R., and Fontes, J.C., 1963, Oxygen isotopic fractionation in the water of crystallization of gypsum: Nature, v. 200, p. 644–646, https://doi.org/10.1038/200644a0.

Groshong, R.H.J., 1975, Strain, fractures, and pressure solution in natural single-layer folds: Geological Society of America Bulletin, v. 86, p. 1363–1376, https://doi.org/10.1130/0016-7606(1975)86<1363:SFAPSI>2.0.CO;2.

Guo, X., Dai, M., Zhai, W., Cai, W.-J., and Chen, B., 2009, CO_2 flux and seasonal variability in a large subtropical estuarine system, the Pearl River Estuary, China: Journal of Geophysical Research–Biogeosciences, v. 114, no. G3, G03013, https://doi.org/10.1029/2008JG000905.

Hancock, P.L., Chalmers, R.M.L., Altunel, E., and Çakir, Z., 1999, Travitonics: Using travertines in active fault studies: Journal of Structural Geology, v. 21, no. 8–9, p. 903–916, https://doi.org/10.1016/S0191-8141(99)00061-9.

Henderson, I.H.C., and McCaig, A.M., 1996, Fluid pressure and salinity variations in shear zone–related veins, central Pyrenees, France: Implications for the fault-valve model: Tectonophysics, v. 262, p. 321–348, https://doi.org/10.1016/0040-1951(96)00018-2.

Holm, P.M., and Munksgaard, N.C., 1982, Evidence for mantle metasomatism: An oxygen and strontium isotope study of the Vulsinian District, central Italy: Earth and Planetary Science Letters, v. 60, no. 3, p. 376–388, https://doi.org/10.1016/0012-821X(82)90074-7.

Kasprzyk, A., and Jasińska, B., 1998, Isotopic composition of the crystallization water of gypsum in the Badenian of the northern Carpathian foredeep: A case study from the cores Przybor6w 1 and Strzegom 143: Geological Quarterly, v. 42, no. 3, p. 301–310.

Lugli, S., 2001, Timing of post-depositional events in the Burano Formation of the Secchia Valley (Upper Triassic, Northern Apennines), clues from gypsum-anhydrite transitions and carbonate metasomatism: Sedimentary Geology, v. 140, p. 107–122.

Lynch, F.L., 1997, Frio shale mineralogy and the stoichiometry of the smectite-to-illite reaction: The most important reaction in clastic sedimentary diagenesis: Clays and Clay Minerals, v. 45, p. 618–631, https://doi.org/10.1346/CCMN.1997.0450502.

Marini, L., and Chiodini, G., 1994, The role of carbon dioxide in the carbonate-evaporite geothermal systems of Tuscany and Latium (Italy): Acta Vulcanologica, v. 5, p. 95–104.

Martinis, B., and Pieri, M., 1964, Alcune notizie sulla formazione evaporitica del Triassico Superiore nell'Italia centrale e meridionale: Memorie della Società Geologica Italiana, v. 4, p. 649–678.

Mason, E., Edmonds, M., and Turchyn, A.V., 2017, Remobilization of crustal carbon may dominate volcanic arc emissions: Science, v. 357, no. 6348, p. 290–294, https://doi.org/10.1126/science.aan5049.

McArthur, J.M., Howarth, R.J., and Bailey, T.R., 2001, Strontium isotope stratigraphy: LOWESS version 3: Best fit to the marine Sr-isotope curve for 0–509 Ma and accompanying look-up table for deriving numerical age: The Journal of Geology, v. 109, p. 155–170, https://doi.org/10.1086/319243.

McArthur, J.M., Howarth, R.J., and Shields, G.A., 2012, Strontium isotope stratigraphy, *in* Gradstein, F.M., Ogg, J.G., Schmitz, M.D., and Ogg, G.M., eds., The Geologic Time Scale: Amsterdam, Elsevier, p. 127–144, https://doi.org/10.1016/B978-0-444-59425-9.00007-X.

McKinley, J.M., Worden, R.H., and Ruffell, A.H., 2013, Smectite in sandstones: A review of the controls on occurrence and behaviour during diagenesis, *in* Worden, R.H., and Morad, S., eds., Clay Mineral Cements in Sandstones: Oxford, UK, Blackwell, p. 109–128.

Mickler, P.J., Banner, J.L., Stern, L., Asmerom, Y., Edwards, R.L., and Ito, E., 2004, Stable isotope variations in modern tropical speleothems: Evaluating equilibrium vs. kinetic isotope effects: Geochimica et Cosmochimica Acta, v. 68, no. 21, p. 4381–4393.

Montanari, A., and Koeberl, C., 2000, Impact Stratigraphy: The Italian Record: Lecture Notes in Earth Sciences 93: Berlin, Springer-Verlag, 364 p.

Nor, A., and Walder, J., 1992, Hydraulic pulses in the Earth's crust, *in* Evans, B., and Wong, T.F., eds., Fault Mechanics and Transport Properties of Rocks; a Festschrift in Honor of W.F. Brace: San Diego, California, Academic Press, p. 461–473, https://doi.org/10.1016/S0074-6142(08)62834-X.

O'Hara, K., and Haak, A., 1992, A fluid inclusion study of fluid pressure and salinity variations in the footwall of the Rector Branch thrust, North Carolina, U.S.A.: Journal of Structural Geology, v. 14, p. 579–589, https://doi.org/10.1016/0191-8141(92)90158-S.

Raven, M.J., and Dickson, J.A.D., 1989, Fir-tree zoning: An indicator of pulsed crystallization in calcite cement crystals: Sedimentary Geology, v. 65, no. 3–4, p. 249–259, https://doi.org/10.1016/0037-0738(89)90027-4.

Rendel, P.M., Gavrieli, I., Wolff-Boenisch, D., and Ganor, J., 2016, Gypsum solubility under pressure conditions relevant to CO_2 geological storage: International Journal of Greenhouse Gas Control, v. 55, p. 15–22, https://doi.org/10.1016/j.ijggc.2016.10.017.

Roland, P., and Ola, K., 1996, Physico/chemical stability of smectite clays: Engineering Geology, v. 41, p. 73–85.

Shackleton, N., 1967, Oxygen isotope analyses and Pleistocene temperatures re-assessed: Nature, v. 215, no. 5096, p. 15–17, https://doi.org/10.1038/215015a0.

Shore, M., and Fowler, A.D., 1996, Oscillatory zoning in minerals; a common phenomenon: Canadian Mineralogist, v. 34, no. 6, p. 1111–1126.

Sibson, R., Moore, R., and Rankin, A., 1975, Seismic pumping—A hydrothermal transport mechanism: Journal of the Geological Society, v. 131, p. 653–659, https://doi.org/10.1144/gsjgs.131.6.0653.

Smalley, P.C., Higgins, A.C., Howarth, R.J., Nicholson, H., Jones, C.E., Swinburne, N.H.M., and Bessa, J., 1994, Seawater Sr isotope variations through time: A procedure for constructing a reference curve to date and correlate marine sedimentary rocks: Geology, v. 22, no. 5, p. 431–434, https://doi.org/10.1130/0091-7613(1994)022<0431:SSIVTT>2.3.CO;2.

Thirlwall, M.F., 1991, Long-term reproducibility of multi-collector Sr and Nd isotope ratio analysis: Chemical Geology, v. 94, p. 85–104.

Turi, B., and Taylor, H.P., 1976, Oxygen isotope studies of potassic volcanic rocks of the Roman Province, central Italy: Contributions to Mineralogy and Petrology, v. 55, no. 1, p. 1–31, https://doi.org/10.1007/BF00372752.

Uysal, I.T., Feng, Y.-x., Zhao, J.-x., Isik, V., Nuriel, P., and Golding, S.D., 2009, Hydrothermal CO_2 degassing in seismically active zones during the late Quaternary: Chemical Geology, v. 265, no. 3–4, p. 442–454, https://doi.org/10.1016/j.chemgeo.2009.05.011.

Van der Pluijm, B.A., and Marshak, S., 2004, Earth Structure: An Introduction to Structural Geology and Tectonics (2nd ed.): New York, W.W. Norton & Company, Inc., 656 p.

Veizer, J., 1983, Chemical diagenesis of carbonates: Theory and application of trace element technique, *in* Arthur, M.A., Anderson, T.F., Kaplan, I.R., Veizer, J., and Land, L.S., eds., Stable Isotopes in Sedimentary Geology: Society of Economic Paleontologists and Mineralogists (SEPM) Short Course 10, p. 3.1–3.100.

Vrolijk, P., 1987, Tectonically driven fluid flow in the Kodiak accretionary complex, Alaska: Geology, v. 15, p. 466–469, https://doi.org/10.1130/0091-7613(1987)15<466:TDFFIT>2.0.CO;2.

Manuscript Accepted by the Society 18 January 2019
Manuscript Published Online xx Month 2019